2014-04

Partially Fluorinated Oxo-Alkoxide Tungsten(VI) Complexes as Precursors for Deposition of WO_x Nanomaterials

UTD AUTHOR(S): Ashley A. Ellsworth and Amy V. Walker

Dalton Transactions

PAPER

View Article Online
View Journal | View Issue

Cite this: *Dalton Trans.*, 2014, **43**, 9226

Partially fluorinated oxo-alkoxide tungsten(VI) complexes as precursors for deposition of WO_x nanomaterials†

Richard O. Bonsu,[a] Hankook Kim,[b] Christopher O'Donohue,[b] Roman Y. Korotkov,[c] K. Randall McClain,[a] Khalil A. Abboud,[a] Ashley A. Ellsworth,[d] Amy V. Walker,[d] Timothy J. Anderson[b] and Lisa McElwee-White*[a]

Received 7th February 2014,
Accepted 29th April 2014

DOI: 10.1039/c4dt00407h

www.rsc.org/dalton

The partially fluorinated oxo-alkoxide tungsten(VI) complexes $WO(OR)_4$ [**4**; R = $C(CH_3)_2CF_3$, **5**; R = $C(CH_3)(CF_3)_2$] have been synthesized as precursors for chemical vapour deposition (CVD) of WO_x nanocrystalline material. Complexes **4** and **5** were prepared by salt metathesis between sodium salts of the fluoroalkoxides and $WOCl_4$. Crystallographic structure analysis allows comparison of the bonding in **4** and **5** as the fluorine content of the fluoroalkoxide ligands is varied. Screening of **5** as a CVD precursor by mass spectrometry and thermogravimetric analysis was followed by deposition of WO_x nanorods.

Introduction

Tungsten oxide nanostructured materials have been studied for several applications, including gas sensing devices[1–3] and anodic charge injection layers for dye-sensitized solar cells (DSSCs).[2,4–6] The interest in WO_x nanomaterials for these applications is due to its strong and selective response to infrared (IR) light. Compared to the commonly used TiO_2, which responds to ultraviolet radiation (UV), the IR absorption by WO_x nanocrystals provides better band gap matching with numerous low lying LUMO infrared absorbing organic dyes used in DSSCs.[5] Additional investigations have demonstrated that the photo-responses of WO_x nanotubes are modified by absorption/desorption of small molecules, which facilitates use of this material in sensors.[1,2,6] In either application, it is observed that an increase in surface area-to-volume ratio of the WO_x nanocrystals leads to significantly improved photosensitivity.[2] It is noted that the stoichiometry and crystalline phase is critical in determining the properties of the material.[7,8]

CVD has been employed for conformal and large surface area growth of WO_x films[9–11] and with appropriate precursors and deposition conditions can enable growth of nanocrystalline materials under moderate reaction conditions. In addition to the possibility of controlling the properties of CVD materials through the structure and decomposition chemistry of precursors,[12–22] aerosol-assisted chemical vapour deposition (AACVD)[23–25] can be carried out in flexible reaction environments that are operated in a range of temperatures and pressures. With a higher mass transport rate of the precursor, the AACVD deposition rate could be several orders of magnitude higher than in CVD methods that rely on precursor volatilization or other techniques that have been used to synthesize WO_x.[2,3,6,7]

Tungsten oxide nanostructures can be prepared by CVD from the volatile carbonyl complex $W(CO)_6$, but a carbon nanotube template or a co-reactant was required.[26] AACVD of WO_3 nanorods from $W(OPh)_6$[24,27] and $W(CO)_6$[28] has also been reported. In addition, tungsten oxo complexes with ancillary aminoalkoxide ligands have been used to prepare WO_x needles by hydrolysis but water is not compatible with some applications.[29]

Given the limited range of established precursors for WO_x nanostructures, we sought to prepare molecular single source precursors that could be suitable for both conventional CVD and AACVD. Good candidates would possess adequate volatility and reactivity to enable oxide growth by CVD at moderate temperatures,[30,31] while being sufficiently soluble and stable in suitable solvents for AACVD. Incorporation of trifluoromethyl

[a]*Department of Chemistry, University of Florida, Gainesville, Florida 32611-7200, USA. E-mail: lmwhite@chem.ufl.edu*
[b]*Department of Chemical Engineering, University of Florida, Gainesville, Florida 32611-6005, USA. E-mail: tim@ufl.edu*
[c]*Arkema Inc., 900 First Ave., King of Prussia, PA 19406, USA*
[d]*Department of Materials Science and Engineering RL10, University of Texas at Dallas, 800 W. Campbell Rd, Richardson, Texas 75080, USA*

†Electronic supplementary information (ESI) available: ^{1}H NMR, ^{19}F NMR and ^{13}C NMR spectra of complexes **4** and **5**. Table of bond distances, bond angles, atomic coordinates, and equivalent isotropic displacement parameters for **4** and **5**. DTA measurements of compounds **1**, **4** and **5**. Thermal behaviours of **1**, **4** and **5** based on TG/DTA measurements. Relative abundances for positive ion DIPCI mass spectra of complexes **4** and **5**. CCDC 985672 and 985673. For ESI and crystallographic data in CIF or other electronic format see DOI: 10.1039/c4dt00407h

groups into sterically bulky alkoxide and beta-diketonate ligands of CVD precursors has been known to impart sufficient volatility.[32–35] The partially fluorinated alkoxide precursor $WO(OCH_2CF_3)_4$ has been reported for atmospheric pressure CVD growth of WO_x,[36] but the synthesis was described as problematic and the depositions produced films, in contrast to the nanorod growth reported here. The potential precursor compound $WO[OC(CH_3)_2CF_3]_4$ (**4**) was first mentioned as a decomposition product during cross-metathesis reactions of the corresponding tungsten alkylidyne and nitriles.[37] We now report an improved synthesis of **4** along with synthesis and characterization of the related volatile complex $WO[OC(CF_3)_2CH_3]_4$ (**5**). Aerosol assisted chemical vapour deposition from **5** results in WO_x nanorod growth.

Experimental details

General procedures

All reactions were carried out under an atmosphere of dry nitrogen using either glovebox or standard Schlenk techniques. All chemicals used were of reagent grade. Methylene chloride, diethyl ether, hexane and toluene from Fisher Scientific were distilled and stored over molecular sieves (4 Å) for at least 48 h prior to experiments. Anhydrous 1,2-dimethoxyethane (Sigma-Aldrich), hexamethyldisiloxane (Sigma-Aldrich) and benzene-d_6 (Cambridge Isotopes) were stored over 4 Å molecular sieves for at least 48 h before use. NaH, WCl_6 (Sigma-Aldrich) and fluorinated *tert*-butanol (SynQuest labs) were used as received. Compounds $WOCl_4$[38] (**1**), $NaOC(CH_3)_2CF_3$ (**2**) and $NaOCCH_3(CF_3)_2$ (**3**)[32,35] were synthesized as reported in their respective literature. NMR spectra were recorded on a Varian Mercury 300BB (300 MHz) spectrometer using residual protons from deuterated solvents for reference. Elemental analysis was conducted by Complete Analysis Laboratory Inc. (Parsippany, NJ). Mass spectrometry was performed on a Thermo Scientific Trace GC DSQ equipped with direct insertion probe (DIP) using chemical ionization (CI) with methane as the reagent gas. The DTA/TGA samples were heated 10 °C min^{-1} to 600 °C. All runs were done under nitrogen using the Mettler TGA/SDTA 851e with a crimped 40 μL aluminium pan. The lid was pierced using the Mettler piercing kit under nitrogen.

Synthesis of $WO[OC(CH_3)_2CF_3]_4$ (4). In the glovebox, $WOCl_4$ (1.46 mmol, 0.500 g) was weighed into a 50 mL Schlenk flask equipped with a stir bar, and 10 mL of 1,2-dimethoxyethane was added to make a suspension. $NaOC(CH_3)_2CF_3$ (5.85 mmol, 0.880 g) was dissolved in 20 mL DME and transferred into an addition funnel. The addition funnel was fitted to the Schlenk flask and brought to the Schlenk line. The contents of the Schlenk flask were stirred and cooled to 0 °C and the DME solution of $NaOC(CH_3)_2CF_3$ was added dropwise for a period of 30 min. The original orange colour changed to greenish-yellow to bluish-grey to yellowish-brown after addition of the two starting materials. The reaction was stirred at 0 °C for another 30 min, after which it was allowed to warm to room temperature and stirred for the next 12 h to obtain a light brownish solution. The reaction mixture was transferred back into the glovebox and the mixture was filtered through a Celite pad to yield a yellowish-brown filtrate. At the Schlenk line, solvent was pulled off under vacuum until a brownish gummy residue remained. The residue was dissolved and stirred in hexane, the solvent was removed and the residue left under vacuum overnight. The light brown powder was sublimed between 85–90 °C (400 mTorr) to yield 0.54 g of a yellowish-white sublimate (52%). The compound was identified by comparison to literature data.[37] Single crystals suitable for X-ray structure determination were grown from toluene at −3 °C.

Synthesis of $WO[OC(CF_3)_2CH_3]_4$ (5). All reaction protocols were the same as for **4** above, starting with $NaOC(CF_3)_2CH_3$ (5.85 mmol, 1.19 g) dissolved in 20 mL DME and $WOCl_4$ (1.46 mmol, 0.500 g) dissolved in 10 mL DME. The orange colour of $WOCl_4$ immediately turned bluish, then pale yellow after addition. The reaction was run at room temperature for 12 h to yield a yellow-brown gummy solid, which was sublimed between 75 and 80 °C (400 mTorr) to yield a pale yellowish sublimate (0.57 g, 48%). ^{1}H NMR (C_6D_6, 25 °C): δ 1.52 (s, CH_3). ^{13}C NMR (C_6D_6, 25 °C): δ 123.75 (q, CF_3, $^1J_{C-F}$ = 287.9 Hz), 87.06 (septet, $C(CF_3)_2CH_3$ $^2J_{C-F}$ = 32.3 Hz), 15.76 (s, CH_3). ^{19}F NMR (C_6D_6, 25 °C): δ −76.25 (s, C(CF_3)$_2$CH$_3$). Anal. calcd for $WO_5C_{16}H_{12}F_{24}$: C, 20.78; H, 1.30. Found: C, 20.74; H, 1.44%. Crystals suitable for X-ray structure determination were grown by cooling a sample dissolved in a solvent mixture of toluene and DMSO to −3 °C.

Crystallographic structure determination of 4 and 5

X-Ray intensity data were collected at 100 K; **4** on a Bruker DUO diffractometer and **5** on a Bruker SMART diffractometer both using Mo Kα radiation (λ = 0.71073 Å) and an APEXII CCD area detector. Raw data frames were read by the program SAINT[39] and integrated using 3D profiling algorithms. The resulting data were reduced to produce *hkl* reflections and their intensities and estimated standard deviations. The data were corrected for Lorentz and polarization effects and numerical absorption corrections were applied based on indexed and measured faces. The structure for **4** was solved and refined in SHELXTL6.1,[40] using full-matrix least-squares refinement. The non-H atoms were refined with anisotropic thermal parameters and all of the H atoms were calculated in idealized positions and refined riding on their parent atoms. The complex **4** is located on a 2-fold rotational axis, thus a half exists in the asymmetric unit. In the final cycle of refinement of **4**, 2652 reflections (of which 2517 are observed with $I > 2\sigma(I)$) were used to refine 159 parameters and the resulting R_1, wR_2 and S (goodness of fit) were 2.02%, 4.32% and 1.040, respectively. The structure for **5** was solved and refined in SHELXTL2013.[41] In the final cycle of refinement of **5**, 93 014 reflections (of which 6573 are observed with $I > 2\sigma(I)$) were used to refine 457 parameters and the resulting R_1, wR_2 and S (goodness of fit) were 2.23%, 5.82% and 1.081, respectively. The refinement was carried out by minimizing the wR_2

function using F^2 rather than F values. R_1 is calculated to provide a reference to the conventional R value but its function is not minimized. The toluene molecules encountered in **5** were disordered and could not be modelled properly, thus the program SQUEEZE,[42] a part of the PLATON[43] package of crystallographic software, was used to calculate the solvent disorder area and remove its contribution to the overall intensity data.

Growth of WO_x nanorods. Compound **5** was tested using a custom AACVD reactor.[44,45] The solid precursor was dissolved in anhydrous diglyme at a concentration of 0.034 M and pumped into a nebulizer at a rate of 4 mL h^{-1}. Nitrogen (99.999% purity, 1000 sccm) was used as carrier gas and the reaction chamber pressure was maintained at 350 Torr. Indium Tin Oxide (ITO, 150 nm) coated borosilicate glass substrates were placed on a graphite susceptor and heated to 450 or 550 °C by a radio frequency (RF) induction heat generator. The reaction time was 150 min.

Characterization of WO_x nanorods. X-Ray photoelectron spectroscopy (XPS, Perkin Elmer PHI5100, PHI Versaprobe II), field emission scanning electron microscopy (FESEM, FEI Nova Nano 430), secondary ion mass spectrometry (ION TOF IV, ION TOF Inc.) and X-ray diffraction (XRD, Panalytical X'pert Pro) were used to identify the composition, thickness, morphology, and film crystallinity. The PHI5100 XPS used a non-monochromatized Al Kα X-ray source ($h\upsilon$ = 1486.6 eV). XPS depth profiles and high resolution XPS were obtained using a monochromatic Al Kα X-ray source and charge neutralization employed (electron and Ar^+ ions). Depth profiles were obtained using a 1 keV Ar^+ ion beam. Static TOF SIMS data were obtained using a 25 keV Bi^+ primary ion beam and electron beam charge neutralization. SIMS data were acquired before and after sputtering the samples with a dc Bi^+ ion beam for 30 s.

Results and discussion

Precursor design

A key strategy in mechanism-based precursor design for AACVD utilization is selection of ligands to fine tune electronic and steric properties of the complexes to induce sufficient solubility in a suitable solvent. Dual use in conventional CVD requires consideration of volatility as well. The neutral monomeric metal complexes of fluoroalkoxides are known to display better solvent solubilisation and higher volatilities than the oligomers that are often encountered in conventional metal alkoxide precursors.[32–34] These effects can be attributed to Coulombic repulsive interactions caused by high electron density in the vicinity of the fluorides.[32,46,47] Moreover, fluoroalkoxides are much bulkier than their hydrocarbon equivalents, and are thus able to effectively shield empty coordination sites and prevent oligomerization.[46] The net effect is expected to be formation of monomeric complexes with sufficient solubility for AACVD applicability and volatility for conventional CVD. Another benefit that could be derived from fluoroalkoxide ligands is the increased acidity of the hydroxylic protons of their corresponding alcohols. For instance, $(CH_3)(CF_3)_2COH$ has a pK_a of approximately 9.0,[32] which could be exploited to simplify the synthetic process through more favourable alcohol exchange or simple salt metathesis.

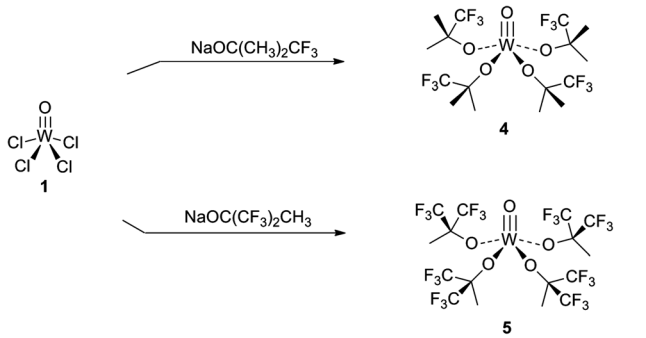

Scheme 1 Synthesis of **4** and **5**.

Synthesis

The synthetic route to **4** and **5** (Scheme 1) parallels a general salt metathesis method previously used by Schrock to isolate a similar compound.[48] Addition of DME solutions of the sodium alkoxide salts **2** and **3**[32,35] to suspensions of **1** in DME was carried out dropwise over 30 min at 0 °C. A series of colour changes observed during slow addition of the two starting materials signified sequential substitution at the tungsten. The brown gummy residues formed upon removal of volatiles from reaction mixtures were purified by sublimation. Complex **4** sublimed between 85 and 90 °C (400 mTorr) as a yellowish-white solid with an average yield of 52%, while complex **5** sublimed between 75 and 80 °C (400 mTorr) as a moist yellowish solid with an average yield of 48%. Precursors **4** and **5** exhibit good solubility in organic solvents, especially in ethers (diethyl ether, THF, monoglyme, diglyme) in which their solubility is more than five-fold higher than the 0.01–0.02 M concentrations that are commonly utilized in AACVD.[28,49]

NMR characterization of 4 and 5

The ^{1}H NMR and ^{19}F NMR spectra of precursors **4**[37] and **5** are consistent with the symmetry equivalence of the hydrogen and the fluorine substituents on the *tert*-butoxide ligands. The methyl groups of **4** and **5** give rise to singlets in the ^{1}H NMR spectra, which exhibit no coupling to the fluorine atoms four bonds away. This is consistent with the ^{19}F NMR spectra, which show singlet peaks for the CF_3 groups. In the ^{13}C NMR spectra, ^{13}C–^{19}F coupling is observed for the CF_3 carbons ($^1J_{CF}$ ≈ 285.6 Hz) and the tertiary carbons ($^2J_{CF}$ ≈ 29.9 Hz) of **4**, whereas these were $^1J_{CF}$ ≈ 287.9 Hz and $^2J_{CF}$ ≈ 32.3 Hz, respectively in **5**.

X-Ray crystal structures of 4 and 5

Single crystals suitable for X-ray diffraction were grown for compounds **4** and **5**, and their geometries were determined to

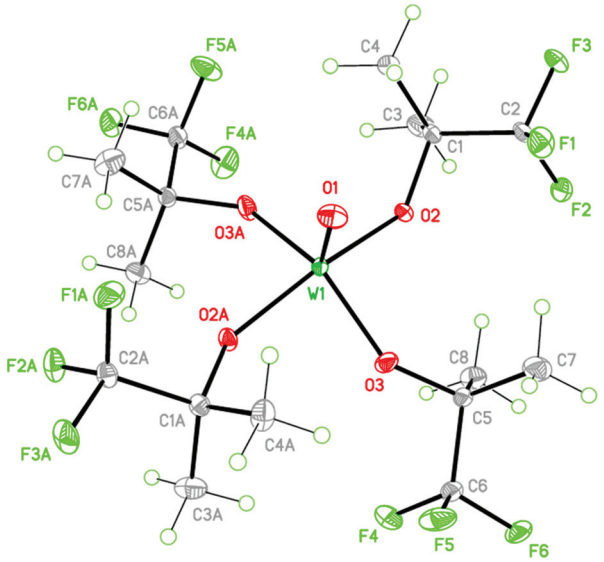

Fig. 1 Displacement ellipsoid diagram of the molecular geometry of **4** drawn at 40% probability.

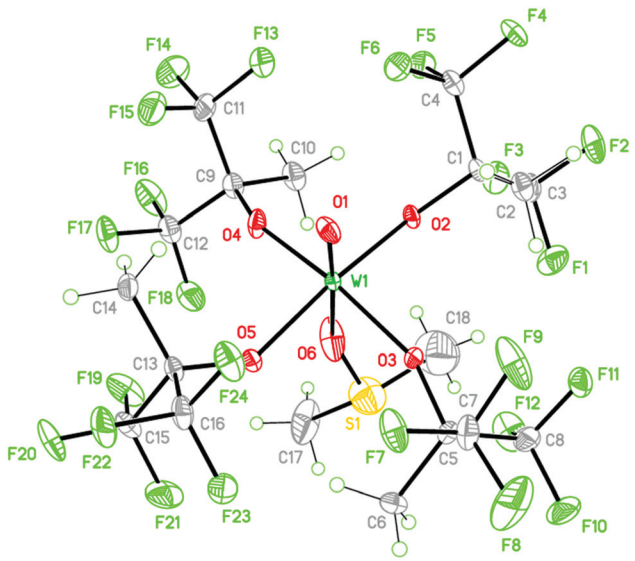

Fig. 2 Displacement ellipsoid diagram of the molecular geometry of **5** with coordinated DMSO drawn at 40% probability.

be monomeric in the solid state (Fig. 1 and 2, Table 1). The coordination geometry of complex **4** was the expected square pyramidal geometry about the tungsten centre (Fig. 1). The oxo ligand occupies the apical position with the four trifluoro-*tert*-butoxide ligands coordinating equatorially, and bent just slightly below the plane of the W(VI) to complete the square pyramid. The W–O bond distance for the terminal oxo ligand of **4** is 1.700(3) Å (Table 2), which is within the range found for similar tungsten complexes with terminal oxo ligands,[50,51] and is suggestive of multiple bonding. In oxoalkoxide compounds such as **4** and **5**, competition from the equatorial alkoxides for the π-orbitals of the metal[50,52] lowers the W–O(oxo) bond order from its maximum value of three.[51,53] The slightly longer W–O terminal bond distance for **4** with respect to the 1.684(4) Å for its precursor $WOCl_4$[54] (**1**) can be attributed to weaker π-bonding capability of the chlorides as compared to the trifluoro-*tert*-butoxide ligands in compound **4**.

The molecular geometry of compound **5** determined by X-ray crystallography shows similarities to that of compound **4**;

Table 1 Crystal data and structure refinement of complexes **4** and **5**

Identification code	**4**	**5**
Formula	$C_{16}H_{24}F_{12}O_5W$	$C_{18}H_{18}F_{24}O_6SW$
Formula weight	708.20	1002.23
Temperature (K)	100(2)	100(2)
Crystal system	Monoclinic	Orthorhombic
Space group	*C*2/*c*	$P2_12_12_1$
a (Å)	20.1356(18)	10.612(3)
b (Å)	6.0103(6)	15.222(5)
c (Å)	20.6144(19)	18.311(6)
β (°)	112.173(2)	90
Z	4	4
Volume (Å^3)	2310.3(4)	2958.0(15)
Density (mg m^{-3})	2.036	2.251
Crystal size (mm^3)	0.16 × 0.13 × 0.08	0.289 × 0.225 × 0.184
Absorption coefficient	5.121 mm^{-1}	4.163 mm^{-1}
F(000)	1368	1920
Index range	$-25 \le h \le 26$, $-7 \le k \le 7$, $-26 \le l \le 25$	$-13 \le h \le 13$, $-19 \le k \le 19$, $-23 \le l \le 23$
Theta range for data coll.	2.13 to 27.50°	1.740 to 27.497°
Independent reflections	2652 [*R*(int) = 0.0267]	6777 [*R*(int) = 0.0346]
Completeness to theta	99.8% (θ = 27.50)	100.0% (θ = 25.242)
GOF on F^2	1.040	1.082
Data/restraints/param.	2652/0/159	6777/0/457
Abs. corr.	Numerical	Numerical
Final *R* indices [$I > 2\sigma(I)$]	R_1 = 0.0202, wR_2 = 0.0432 [2517]	R_1 = 0.0223, wR_2 = 0.0582 [6573]
R indices (all data)	R_1 = 0.0223, wR_2 = 0.0441	R_1 = 0.0233, wR_2 = 0.0586
Largest diff peak and hole	3.774 and −0.897 e Å^{-3}	0.981 and −1.752 e Å^{-3}

$R_1 = \sum(||F_o| - |F_c||)/\sum|F_o|$.w$R_2 = [\sum[w(F_o^2 - F_c^2)^2]/\sum(w(F_o^2)^2]]^{1/2}$.$S = [\sum[w(F_o^2)^2 - F_c^2)^2]/(n-p)]^{1/2}$.w = $1/[\sigma^2(F_o^2) + (mp)^2 + np]$, $p = [\max(F_o^2,0) + 2F_c^2]/3$, *m* & *n* are constants.

Table 2 Selected bond distances (Å) and angles (°) for compounds **4** and **5**

Bond parameter	**4**	Bond parameter	**5**
W1–O1	1.700(3)	W1–O1	1.695(4)
W1–O2	1.8995(18)	W1–O2	1.927(4)
W1–O3	1.8718(19)	W1–O3	1.888(5)
W1–O2A	1.8995(18)	W1–O5	1.927(4)
W1–O3A	1.8718(19)	W1–O4	1.888(5)
O2–W1–O3	87.33(8)	O2–W1–O3	88.6(2)
O3–W1–O2A	86.82(8)	O3–W1–O5	89.3(2)
O2A–W1–O3A	87.33(8)	O5–W1–O4	89.2(2)
O3A–W1–O2	86.82(8)	O4–W1–O2	89.0(2)
O1–W1–O2	98.70(6)	O1–W1–O2	96.8(2)
O1–W1–O3	109.74(7)	O1–W1–O3	99.6(2)
O1–W1–O2A	98.70(6)	O1–W1–O4	98.5(2)
O1–W1–O3A	109.74(7)	O1–W1–O5	95.8(2)

however, **5** exhibits pseudo-octahedral geometry at the tungsten centre due to coordination of DMSO from the crystallization solvent *trans* to the oxo ligand (Fig. 2). The bond angles between the equatorial ligands increase slightly in compound **5**, approaching 90° as a result of the coordinated DMSO and the increased steric bulk in the equatorial ligands of **5**. Moreover, there is slight increase in the W–O(alkoxide) bond distances with the increased fluorination of **5**, which decreases π-donation from the coordinated fluoroalkoxide. The decreased π-donation from the hexafluoro-*tert*-butoxide in **5** is compensated by strong donation from the apical oxo ligand, as evidenced by the shorter W–O(oxo) bond distance of 1.690 (3) Å in **5** as compared with 1.700(3) Å in **4** (Table 2).

Thermal analysis of 4 and 5

The thermogravimetric (TGA) and the differential thermal (DTA) analyses of complexes **4** and **5** (Fig. 3 and Fig. S-7†) demonstrate similar thermal behaviour. Compound **5** volatilizes slightly more readily in the low temperature range (<200 °C). The TGA traces of both complexes show substantial mass loss between 150 and 250 °C through thermal vaporization (Table S-1†). However, there is slight decomposition shown by residual masses of 13.6 and 14.2% for **4** and **5**, respectively, which are constant above 300 °C. The DTA traces in Fig. S-7† present large endotherms at about 105 °C and 100 °C for complexes **4** and **5**, which represent the respective melting points of these compounds.

The phase changes prior to the onset of vaporization are a good indication of their volatility,[55] which is desirable in precursors for CVD. The TGA/DTA traces of both **4** and **5** are compared to that of the starting material **1** ($WOCl_4$), which is also a common WO_x deposition precursor.[56–58] As compared to this material, fluorinated alkoxide derivatives of W^{VI} represent considerable improvement. They have cleaner evaporation as compared to their precursor **1**, which predominantly undergoes thermal decomposition above 200 °C (Fig. 3).

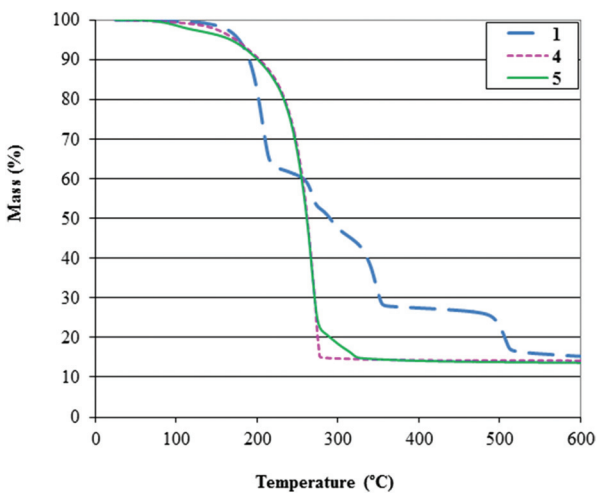

Fig. 3 TGA measurements of compounds **1**, **4** and **5**.

Mass spectrometry of 4 and 5

Fragmentation patterns from mass spectrometry have been correlated with possible gas phase decomposition pathways in a CVD reactor, although it must be taken into consideration that this CVD process does not involve ionization.[59–61] Selected fragments observed in the mass spectra of **4** and **5** in the positive-ion direct insertion probe chemical ionization (DIPCI) mode are summarized in Table 3.

The molecular ions were observed only in small amounts (<10%) for both complexes **4** and **5**. The fragmentation patterns in the mass spectra provide evidence of loss of fluoroalkoxide fragments to give rise to $[WO(OC(CH_3)_2CF_3)_3]^+$ and $[WO(OC(CF_3)_2CH_3)_3]^+$ with peaks at *m*/*z* 581 and 743 from **4** and **5**, respectively. This is supported by the presence of high intensity peaks at *m*/*z* 127 and 129 corresponding to $[OC(CH_3)_2CF_3]^+$ and $[HOC(CH_3)_2CF_3 + H]^+$ from **4** and at *m*/*z* 181 and 183 corresponding to $[OC_4H_3F_6]^+$ and $[HOC_4H_3F_6 + H]^+$ from **5**. The resulting residues undergo subsequent C–O bond cleavage, releasing fluorocarbon fragments to produce peaks for $[WO(OC(CH_3)_2CF_3)_2(OH)(H_2O)]^+$ and $[WO(OC(CF_3)_2CH_3)_2(OH)]^+$ at *m*/*z* 489 and 579 in compounds **4** and **5**, respectively.

These results are consistent with the observation of loss of isobutylene and water upon pyrolysis of $M[OSi(OtBu)_3]_4$ (M = Ti, Zr, Hf) complexes by Tilley.[62,63] A related pathway during fragmentation of **4** and **5** would generate hydroxide ligands in the fragment ions, as well as the fluoroisobutylene ions $[H_2CCH_3CF_3]^+$ and $[H_2CC(CF_3)_2]^+$, which are observed as moderately intense peaks at *m*/*z* 110 and 164 in the mass spectra of **4** and **5**, respectively. Under positive-ion chemical ionization conditions, the hydroxide ligands are likely to be protonated to form aquo ligands, as observed.

Apparent loss of a fluoroalkyl group to generate an oxo ligand has also been observed during the metathesis of nitriles by $EtC{\equiv}W(OCMe_2CF_3)_3$.[37] If fragments observed in the DIPCI-MS are indicative of the gas phase decomposition of compounds **4** and **5**, then successive cleavage of W–O and

Table 3 Summary of relative abundances for positive ion DIPCI mass spectra of complexes **4** and **5**[a]

Compound	Ion	*m*/*z*	Rel. abundance (%)
4	$[M]^+$	708	0.05
	$[WO(OC(CH_3)_2CF_3)_3]^+$	581	2
	$[WO(OC(CH_3)_2CF_3)_2(OH)(H_2O)]^+$	489	1
	$[HOC(CH_3)_2CF_3 + H]^+$	129	33
	$[C(CH_3)_2CF_3]^+$	111	12
	$[H_2CCCH_3CF_3]^+$	110	9
	$[HCCCH_3CF_3]^+$	109	100
5	$[M]^+$	924	9
	$[WO(OCCH_3(CF_3)_2)_3]^+$	743	9
	$[WO(OCCH_3(CF_3)_2)_2(OH)]^+$	579	12
	$[HOC_4H_3F_6 + H]^+$	183	100
	$[H_2CC(CF_3)_2]^+$	164	5
	$[HCC(CF_3)_2]^+$	163	51
	$[H_2C(CF_3)_2]^+$	152	39

[a] Relative abundances were predicted by adjusting peak intensities relative to the highest peak normalized to 100%.

O–C bonds is a viable pathway for decomposition of **4** and **5** to form WO_x films under CVD conditions.

Materials characterization

The grown tungsten oxide materials have a dark-blue colour. As the deposition temperature increases the materials become non-transparent and contain more carbon impurity. The XPS of as-grown material shows 36.0 and 41.9 at% carbon contamination on surfaces of materials grown at 450 and 550 °C, respectively. Additional XPS data were collected after 10 min and 20 min of 500 eV Ar^+ ion sputtering to remove surface contamination. Comparison of composition data between 10 min and 20 min sputtering shows preferred sputtering. After sputtering, more tungsten, and less oxygen and carbon were detected, however, the maximum composition difference between sputtering times was 4.2 at%. Data from XPS after 10 min Ar ion sputtering (Fig. 4 and Table 4) clearly show the material grown by AACVD was tungsten oxide with incorporated carbon. The XPS W 4f, O 1s, and C 1s peaks were deconvoluted after Shirley baseline subtraction. The XPS multiplex survey in Fig. 4 is consistent with $4f_{5/2}$ and $4f_{7/2}$ doublets of tungsten in the W^{6+} and W^{5+} oxidation states.[64–67] Metallic tungsten (W) and tungsten carbide (WC) components were not observed. Carbon peak deconvolution yields signals for free carbon and carbon bonded to oxygen with BE values at 284.4 eV and 285.4 eV, respectively.[65,66,68] The O 1s peak with a BE at 530.7 eV is from WO_x [68–70] and a smaller peak at 531.7 eV arises from oxygen bound to carbon.[66,68] Minor signals from indium and tin are attributed to exposed portions of the ITO substrates. No fluorine peaks were detected in the XPS detection limit, 1 at%, either before or after sputtering. Further, XPS depth profiles (Fig. S8, ESI†) indicate that there is no F present throughout the deposited layer. The oxygen to tungsten ratio increases from 2.56 to 2.94 upon increasing the deposition temperature from 450 to 550 °C. These data suggest that the grown material consists mostly of substoichiometric WO_x with lesser amounts of a C–O containing material, for example, amorphous carbon with chemisorbed oxygen.

TOF SIMS spectra (Fig. S-9 to S-12, ESI†) are consistent with the XPS data. Ions of the form $WO_x^{\pm}$, such as WO_3^-, are observed indicating that WO_x has been deposited. Before and after sputtering of the surface, the intensity of the F^- ion is negligible indicating that there is little, or no, incorporation of F in the deposit. The data also suggest that there is incorporation of carbon and hydrocarbon species in the film especially in the surface region; in the spectra $W_xC_yH_z^{\pm}$ ions, *e.g.* $[WC_4H_6]^+$ are observed.

As shown in the SEM images in Fig. 5, the tungsten oxide deposited at 450 and 550 °C consists of whisker-type nanorod structures. It is apparent from this plan-view SEM image that the nanorod structure in the sample grown at 450 °C shows multiple bundles of several nanorods each, while growth at 550 °C produces unbundled nanorods that are considerably longer and smaller diameter. The nanorods grown at 550 °C are up to 3 μm in length and 20 to 50 nm in diameter, while the nanorods in the bundles grown at 450 °C are ~0.3 μm in length and 50 to 100 nm in diameter. The cross-sectional SEM images in Fig. 5 show that the height of nanorods grown at 450 and 550 °C are 0.3 (±0.02) μm and 2.7 (±0.3) μm, respectively. The XRD spectra in Fig. 6 indicate that materials grown at both temperatures possess the $W_{18}O_{49}$ monoclinic crystal structure. It was observed that the underlying ITO substrate

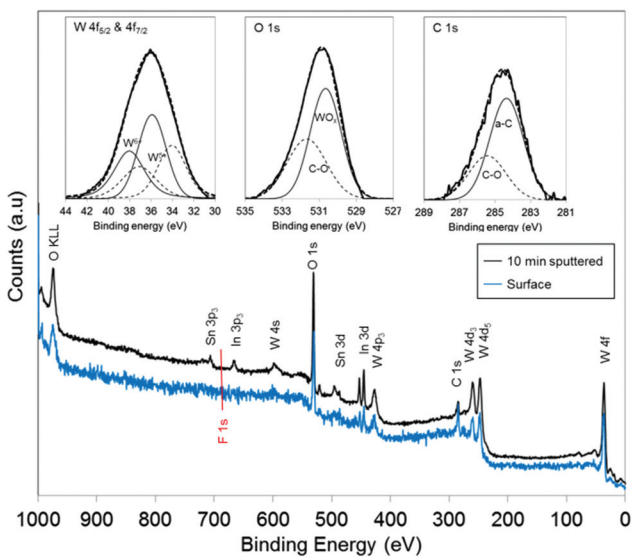

Fig. 4 XPS scan for the film grown from **5** at 550 °C, and multiplex survey of W $4f_5$ and $4f_7$, O 1s, and C 1s (inset: dashed lines and thin solid lines are deconvoluted peaks).

Table 4 XPS atomic compositional data of materials grown from **5**[a]

Deposition temperature (°C)	W (atom%)	O (atom%)	C (atom%)	In (atom%)	Sn (atom%)
450	23.2	62.7	11.8	2.1	0.2
550	19.1	60.8	17.0	2.9	0.2

[a] Data were obtained after 10 min Ar ion sputtering.

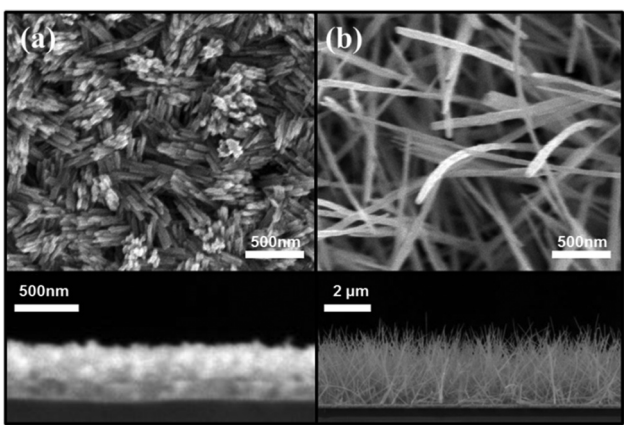

Fig. 5 Plan-view and cross-sectional SEM images of materials grown from **5** at (a) 450, and (b) 550 °C.

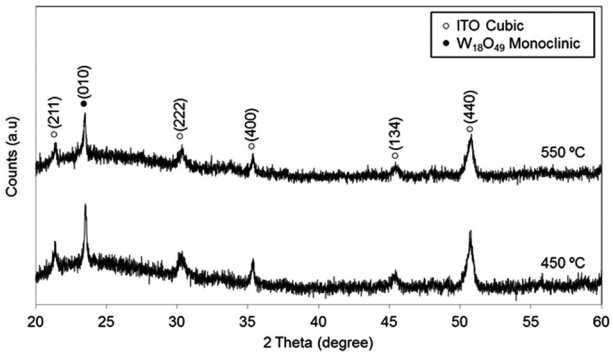

Fig. 6 XRD spectra of materials grown from **5** at 450 and 550 °C.

did not recrystallize or undergo preferential texturing during material depositions. The diffraction peak at 23.5° 2θ corresponds to the $W_{18}O_{49}$ (010) plane, which indicates that the nanorods grow in the [010] direction. This is expected since the {010} planes are the close-packed planes and have the highest surface energy.[71–73]

Boettcher has reported growth of nanorod structures by vapour transport[74] with the same nanorod orientation and similar morphology and stoichiometry to the structure grown using compound **5** at 550 °C (Fig. 5b). Nanorod growth was attributed to the formation of oxygen-deficient planar defects nucleating and serving as preferential sites for 1D growth. Although their films were grown at higher temperature and on a reducing substrate (W-coated Si *vs.* ITO), a similar mechanism may be operative here. Additional studies to address the growth mechanism from **5** are planned.

Conclusions

We have successfully synthesized monomeric neutral oxo-fluoroalkoxide tungsten(VI) complexes $WO(OR)_4$ [**4**; R = C-$(CH_3)_2CF_3$, **5**; R = $C(CF_3)_2CH_3$] by reacting the sodium salts of the bulky fluoroalkoxide ligands with $WOCl_4$. Sublimation of the crude products yields clean solids that can be subsequently crystallized to yield high purity products. Data from crystallographic structure determination indicate increased strength of the apical W–O bond from **4** to **5** as the donor strength of the equatorial fluoroalkoxide ligands decreases with increasing fluorine content. Pre-screening using TGA/DTA suggests both complexes are sufficiently volatile to be promising single source precursors for CVD of WO_x thin films. High temperature AACVD film growth with complex **5** demonstrated growth of WO_x nanorods without an oxygen-containing co-reactant.

Acknowledgements

We thank the National Science Foundation for support under the GOALI grant CHE-1213965. K. A. A. acknowledges the National Science Foundation and the University of Florida for funding the purchase of the X-ray equipment. We would also like to thank the Major Analytical Instrumentation Center of the Engineering Department at the University of Florida for providing and maintaining materials characterization instruments. We also thank Prof. John Gorden for helpful discussion.

Notes and references

1 M. Furubayashi, K. Nagato, H. Moritani, T. Hamaguchi and M. Nakao, *Microelectron. Eng.*, 2010, **87**, 1594–1596.
2 C. Gopalakrishnan, K. Ganesh, S. Ramaswamy and K. Jeganathan, *Mater. Lett.*, 2011, **65**, 1941–1944.
3 Y. Baek and K. Yong, *J. Phys. Chem. C*, 2007, **111**, 1213–1218.
4 A. Z. Sadek, H. D. Zheng, M. Breedon, V. Bansal, S. K. Bhargava, K. Latham, J. M. Zhu, L. S. Yu, Z. Hu, P. G. Spizzirri, W. Wlodarski and K. Kalantar-zadeh, *Langmuir*, 2009, **25**, 9545–9551.
5 K. Hara, Z.-G. Zhao, Y. Cui, M. Miyauchi, M. Miyashita and S. Mori, *Langmuir*, 2011, **27**, 12730–12736.
6 Y. Xie, F. Cheong, B. Varghese, Y. Zhu, R. Mahendiran and C. Sow, *Sens. Actuators, B*, 2011, **151**, 320–326.
7 S. Fukuzumi and Y. Yamada, *J. Mater. Chem.*, 2012, **22**, 24284–24296.
8 A. Baserga, V. Russo, F. Di Fonzo, A. Bailini, D. Cattaneo, C. S. Casari, A. Li Bassi and C. E. Bottani, *Thin Solid Films*, 2007, **515**, 6465–6469.
9 R. U. Kirss and L. Meda, *Appl. Organomet. Chem.*, 1998, **12**, 155–160.
10 R. G. Palgrave and I. P. Parkin, *New J. Chem.*, 2006, **30**, 505–514.
11 I. P. Parkin and R. G. Palgrave, in *Chemical Vapour Deposition*, ed. A. C. Jones and M. L. Hitchman, RSC Publishing, Cambridge, 2009, pp. 451–476.
12 L. McElwee-White, *Dalton Trans.*, 2006, 5327–5333.
13 L. McElwee-White, J. Koller, D. Kim and T. J. Anderson, *ECS Trans.*, 2009, **25**, 161–171.
14 A. Devi, *Coord. Chem. Rev.*, 2013, **257**, 3332–3384.
15 O. Just, B. Obi-Johnson, J. Matthews, D. Levermore, T. Jones and W. S. Rees Jr., *Mater. Res. Soc. Symp. Proc.*, 2000, **606**, 3–12.
16 L. G. Hubert-Pfalzgraf, *J. Mater. Chem.*, 2004, **14**, 3113–3123.
17 C. H. Winter, W. Zheng and H. M. El-Kaderi, in *Encyclopedia of Inorganic Chemistry*, Wiley, Chichester, 2nd edn, 2005, vol. 5, pp. 3121–3144.
18 W. S. Rees Jr., H. A. Luten and V. L. Goedken, *Mater. Res. Soc. Symp. Proc.*, 1995, **363**, 195–206.
19 L. G. Hubert-Pfalzgraf, *Inorg. Chem. Commun.*, 2003, **6**, 102–120.
20 J. O. Carlsson, *Acta Chem. Scand.*, 1991, **45**, 864–869.
21 M. A. Malik and P. O'Brien, in *Chemical Vapour Deposition: Precursors, Processes and Applications*, Royal Society of Chemistry, 2009, pp. 207–271.
22 S. Mathur, H. Shen, E. Hemmer, T. Ruegamer and C. Holzapfel, *Mater. Res. Soc. Symp. Proc.*, 2005, **848**, 55–60.
23 P. Marchand, I. A. Hassan, I. P. Parkin and C. J. Carmalt, *Dalton Trans.*, 2013, **42**, 9406–9422.

24 F. E. Annanouch, S. Vallejos, T. Stoycheva, C. Blackman and E. Llobet, *Thin Solid Films*, 2013, **548**, 703–709.
25 X. Hou and K. L. Choy, *Chem. Vap. Deposition*, 2006, **12**, 583–596.
26 J. Yu, K. H. Choo, L. Niu and D. H. C. Chua, *Electrochem. Solid-State Lett.*, 2011, **14**, K58.
27 S. Vallejos, P. Umek and C. Blackman, *J. Nanosci. Nanotechnol.*, 2011, **11**, 8214–8220.
28 S. Ashraf, C. S. Blackman, R. G. Palgrave and I. P. Parkin, *J. Mater. Chem.*, 2007, **17**, 1063–1070.
29 H. Choujaa, A. L. Johnson, G. Kociok-Kohn and K. C. Molloy, *Dalton Trans.*, 2012, **41**, 11393–11401.
30 A. C. Jones, *J. Mater. Chem.*, 2002, **12**, 2576–2590.
31 A. C. Jones, H. C. Aspinall and P. R. Chalker, *Surf. Coat. Technol.*, 2007, **201**, 9046–9054.
32 J. A. Samuels, E. B. Lobkovsky, W. E. Streib, K. Folting, J. C. Huffman, J. W. Zwanziger and K. G. Caulton, *J. Am. Chem. Soc.*, 1993, **115**, 5093–5094.
33 V. Mazumder, Y. Lee and S. Sun, *Adv. Funct. Mater.*, 2010, **20**, 1224–1231.
34 L. A. Miinea, S. Suh and D. M. Hoffman, *Inorg. Chem.*, 1999, **38**, 4447–4454.
35 J. A. Samuels, K. Folting, J. C. Huffman and K. G. Caulton, *Chem. Mater.*, 1995, **7**, 929–935.
36 K. C. Molloy and P. A. Williams, *Appl. Organomet. Chem.*, 2008, **22**, 560–564.
37 A. M. Geyer, E. S. Wiedner, J. B. Gary, R. L. Gdula, N. C. Kuhlmann, M. J. A. Johnson, B. D. Dunietz and J. W. Kampf, *J. Am. Chem. Soc.*, 2008, **130**, 8984–8999.
38 F. S. Pedersen and R. R. Schrock, *J. Am. Chem. Soc.*, 1982, **104**, 7483–7491.
39 A. Corma, P. Concepción, M. Boronat, M. J. Sabater, J. Navas, M. J. Yacaman, E. Larios, A. Posadas, M. A. López-Quintela, D. Buceta, E. Mendoza, G. Guilera and A. Mayoral, *Nat. Chem.*, 2013, **5**, 775–781.
40 *SHELXTL6*, Bruker-AXS, Madison, Wisconsin, 2008.
41 *SHELXTL2013*, Bruker-AXS, Madison, Wisconsin, 2013.
42 P. van der Sluis and A. L. Spek, *Acta Crystallogr., Sect. A: Fundam. Crystallogr.*, 1990, **46**, 194–201.
43 A. L. Spek, *Acta Crystallogr., Sect. D: Biol. Crystallogr.*, 2009, **65**, 148–155.
44 K. R. McClain, C. O'Donohue, Z. Shi, A. V. Walker, K. A. Abboud, T. Anderson and L. McElwee-White, *Eur. J. Inorg. Chem.*, 2012, **2012**, 4579–4584.
45 O. J. Bchir, S. W. Johnston, A. C. Cuadra, T. J. Anderson, C. G. Ortiz, B. C. Brooks, D. H. Powell and L. McElwee-White, *J. Cryst. Growth*, 2003, **249**, 262–274.
46 W. A. Herrmann, N. W. Huber and O. Runte, *Angew. Chem., Int. Ed. Engl.*, 1995, **34**, 2187–2206.
47 W. D. Buchanan, M. A. Guino-O and K. Ruhlandt-Senge, *Inorg. Chem.*, 2010, **49**, 7144–7155.
48 H. J. Wengrovius and R. R. Schrock, *Organometallics*, 1982, **1**, 148–155.
49 K. C. Molloy and P. A. Williams, *Appl. Organomet. Chem.*, 2008, **22**, 676–683.
50 W. Clegg, J. R. Errington, P. Kraxner and C. Redshaw, *J. Chem. Soc., Dalton Trans.*, 1992, 1431–1438.
51 W. A. Nugent and J. M. Mayer, *Metal-Ligand Multiple Bonds*, Wiley, New York, 1988.
52 M. H. Chisholm, *Polyhedron*, 1983, **2**, 681.
53 R. H. Holm, *Chem. Rev.*, 1987, **87**, 1401–1449.
54 K. Iijima and S. Shibata, *Chem. Lett.*, 1972, 1033–1036.
55 B. W. Cross, P. I. Parkin, J. P. A. White and J. D. Williams, *Dalton Trans.*, 2005, 1287–1293.
56 G. R. Palgrave and P. I. Parkin, *New J. Chem.*, 2006, **30**, 505–561.
57 G. Dai, M. L. Hitchman and S. H. Shamlian, *Adv. Sci. Technol.*, 1995, **5**, 407–414.
58 S. O'Neill, I. P. Parkin, R. J. H. Clark, A. Mills and N. Elliott, *Chem. Vap. Deposition*, 2004, **10**, 136–141.
59 O. J. Bchir, K. M. Green, H. M. Ajmera, E. A. Zapp, T. J. Anderson, B. C. Brooks, L. L. Reitfort, D. H. Powell, K. A. Abboud and L. McElwee-White, *J. Am. Chem. Soc.*, 2005, **127**, 7825–7833.
60 T. S. Lewkebandara, P. H. Sheridan, M. J. Heeg, A. L. Rheingold and C. H. Winter, *Inorg. Chem.*, 1994, **33**, 5879–5889.
61 C. C. Amato, J. B. Hudson and L. V. Interrante, *Mater. Res. Soc. Symp. Proc.*, 1990, **168**, 119–124.
62 K. W. Terry, P. K. Ganzel and T. D. Tilley, *Chem. Mater.*, 1992, **4**, 1290–1295.
63 K. W. Terry and T. D. Tilley, *Chem. Mater.*, 1991, **3**, 1001–1003.
64 G. Wang, Y. Ling, H. Wang, X. Yang, C. Wang, J. Z. Zhang and Y. Li, *Energy Environ. Sci.*, 2012, **5**, 6180–6187.
65 A. Katrib, F. Hemming, P. Wehrer, L. Hilaire and G. Maire, *Top. Catal.*, 1994, **1**, 75–85.
66 Y.-S. Lin, H.-T. Chen and S.-S. Wu, *J. Solid State Electrochem.*, 2010, **14**, 1885–1895.
67 R. L. Stewart, *Phys. Rev.*, 1934, **45**, 488–490.
68 P. Delporte, F. Meunier, C. Phamhuu, P. Vennegues, M. J. Ledoux and J. Guille, *Catal. Today*, 1995, **23**, 251–267.
69 L. Salvati, L. E. Makovsky, J. M. Stencel, F. R. Brown and D. M. Hercules, *J. Phys. Chem.*, 1981, **85**, 3700–3707.
70 K. Edinger, H. Becht, J. Bihr, V. Boegli, M. Budach, T. Hofmann, H. W. P. Koops, P. Kuschnerus, J. Oster, P. Spies and B. Weyrauch, *J. Vac. Sci. Technol., B*, 2004, **22**, 2902–2906.
71 G. Gu, B. Zheng, W. Q. Han, S. Roth and J. Liu, *Nano Lett.*, 2002, **2**, 849–851.
72 T. Liang, E. Frendberg, B. Lieberman and A. Stivers, *J. Vac. Sci. Technol., B*, 2005, **23**, 3101–3105.
73 C. T. H. Heerkens, M. J. Kamerbeek, W. F. van Dorp, C. W. Hagen and J. Hoekstra, *Microelectron. Eng.*, 2009, **86**, 961–964.
74 A. M. Smith, M. G. Kast, B. A. Nail, S. Aloni and S. W. Boettcher, *J. Mater. Chem. A*, 2014, **2**, 6121–6129.

Supporting Information for:

Partially Fluorinated Oxo-alkoxide Tungsten (VI) Complexes as Precursors for Deposition of WO_x Nanomaterials

Richard O. Bonsu,[a] *Hankook Kim,*[b] *Christopher O'Donohue,*[b] *Roman Y. Korotkov,*[c] *K. Randall McClain,*[a] *Khalil A. Abboud,*[a] *Ashley A. Ellsworth,*[d] *Amy V. Walker,*[d] *Timothy J. Anderson*[b] *and Lisa McElwee-White*[*,a]

[a]Department of Chemistry, University of Florida, Gainesville, Florida, 32611-7200 USA. Email: lmwhite@chem.ufl.edu

[b]Department of Chemical Engineering, University of Florida, Gainesville, Florida, 32611-6005 USA

[c]Arkema Inc., 900 First Ave., King of Prussia, PA 19406 USA

[d]Department of Materials Science and Engineering RL10, University of Texas at Dallas, 800 W. Campbell Rd, Richardson, Texas 75080 USA

lmwhite@chem.ufl.edu
tim@ufl.edu

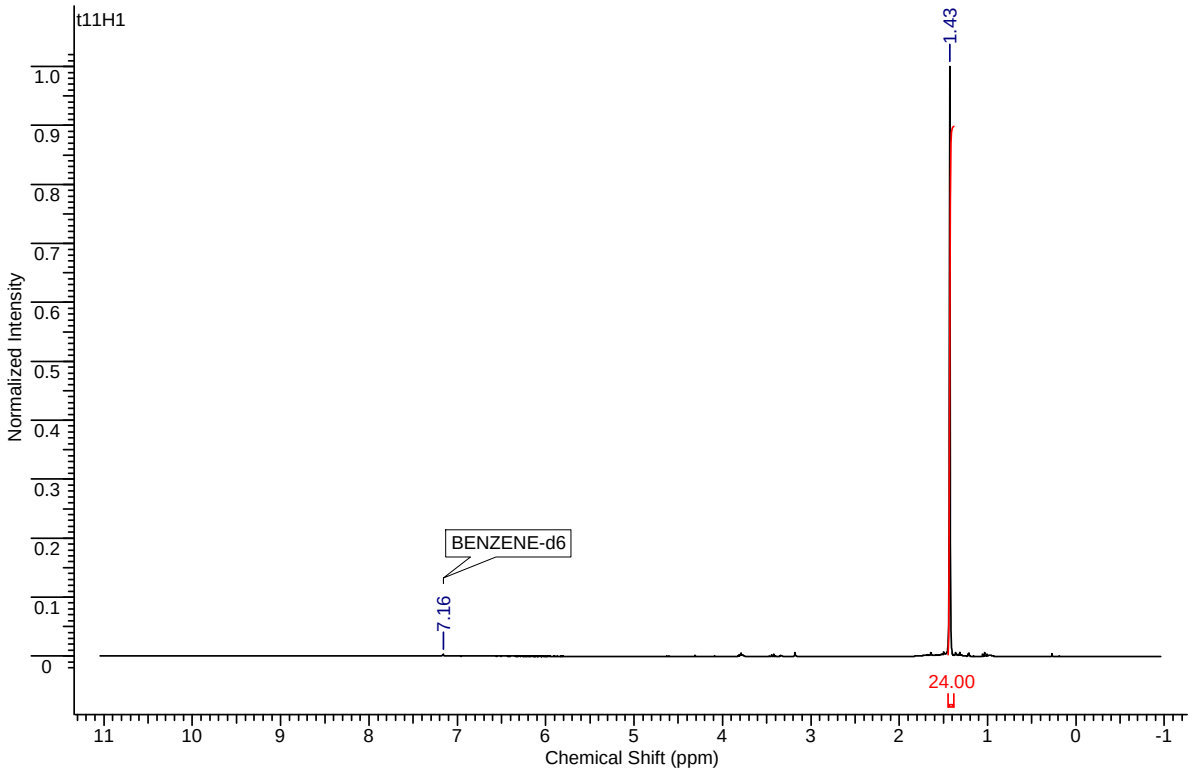

Figure S-1: Room Temperature ^{1}H NMR of **4** in benzene-d_6.

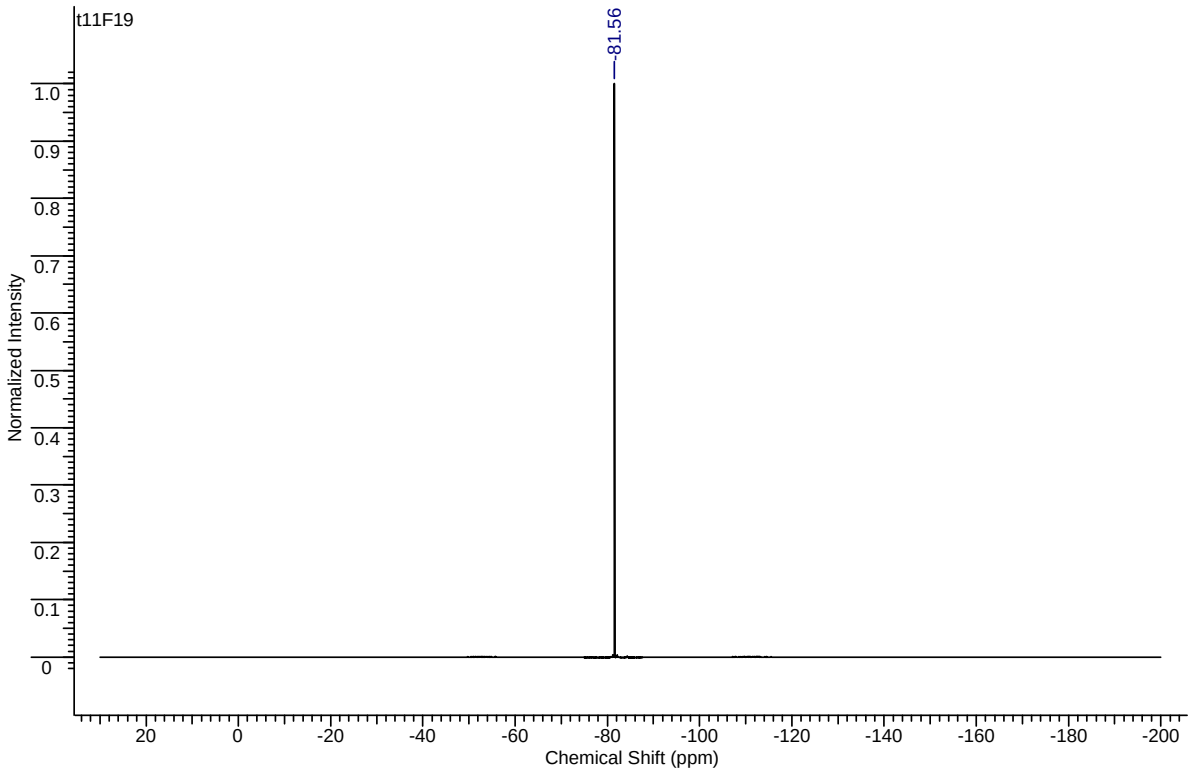

Figure S-2: Room Temperature ^{19}F NMR of **4** in benzene-d_6.

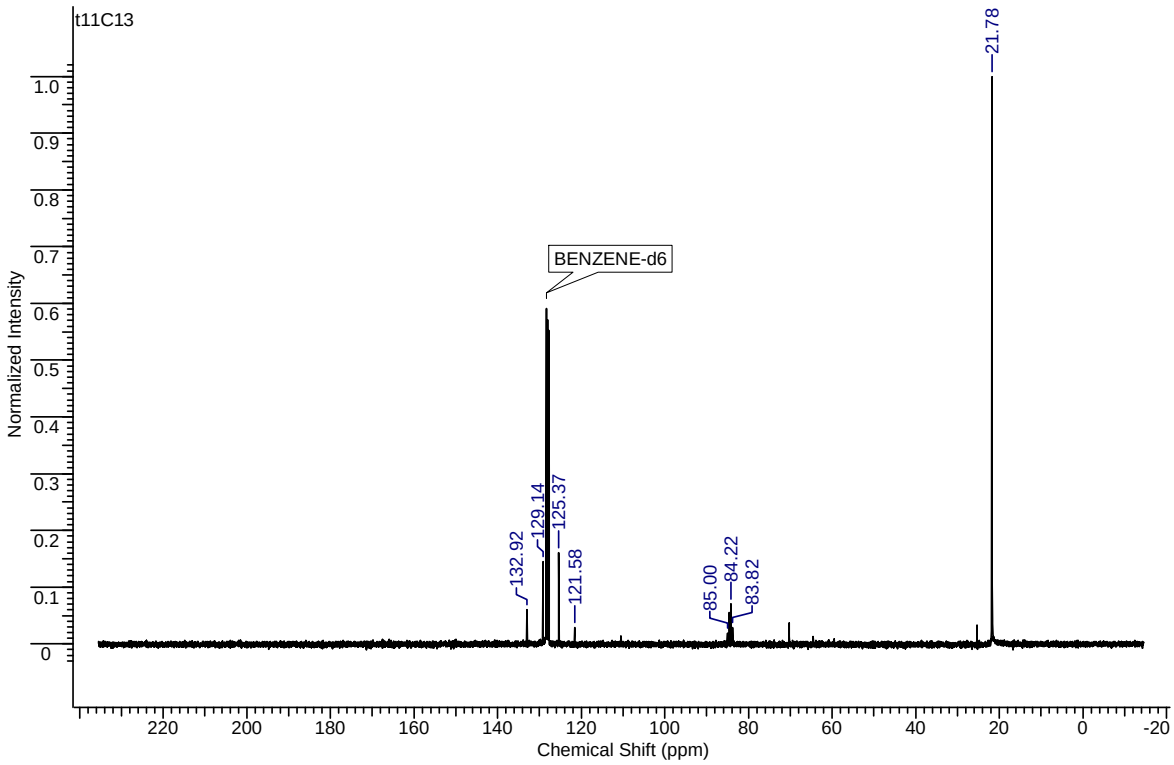

Figure S-3: Room Temperature ^{13}C NMR of **4** in benzene-d_6.

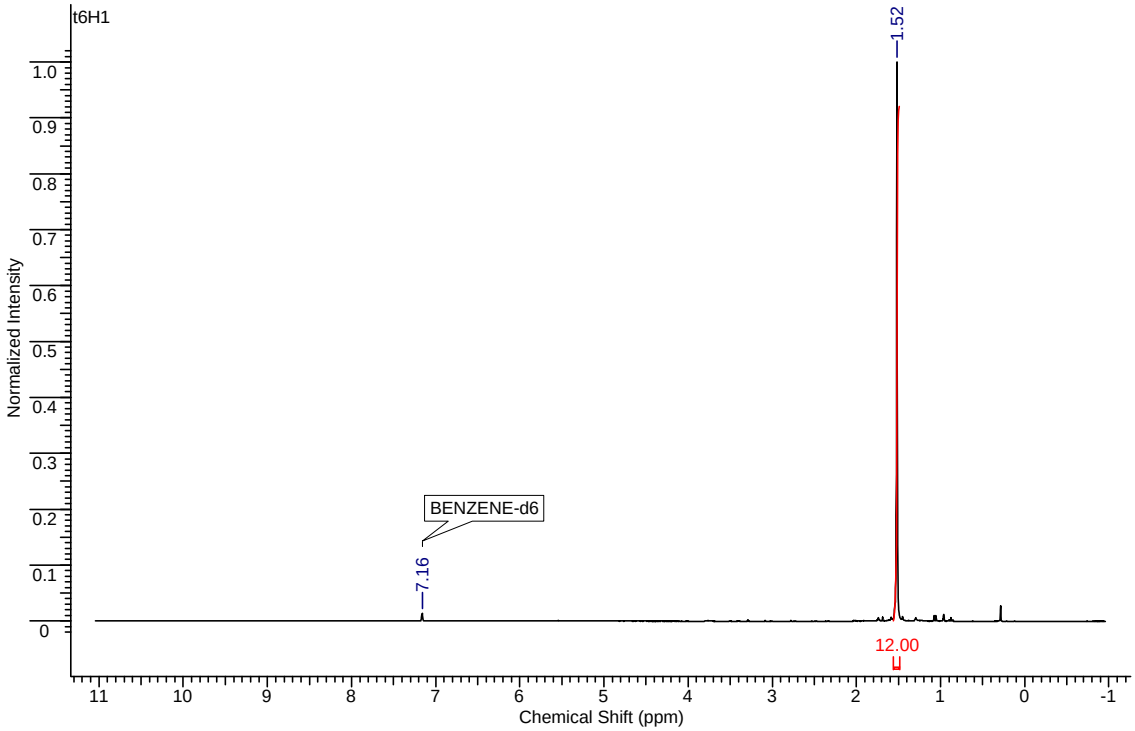

Figure S-4: Room Temperature ^{1}H NMR of **5** in benzene-d_6.

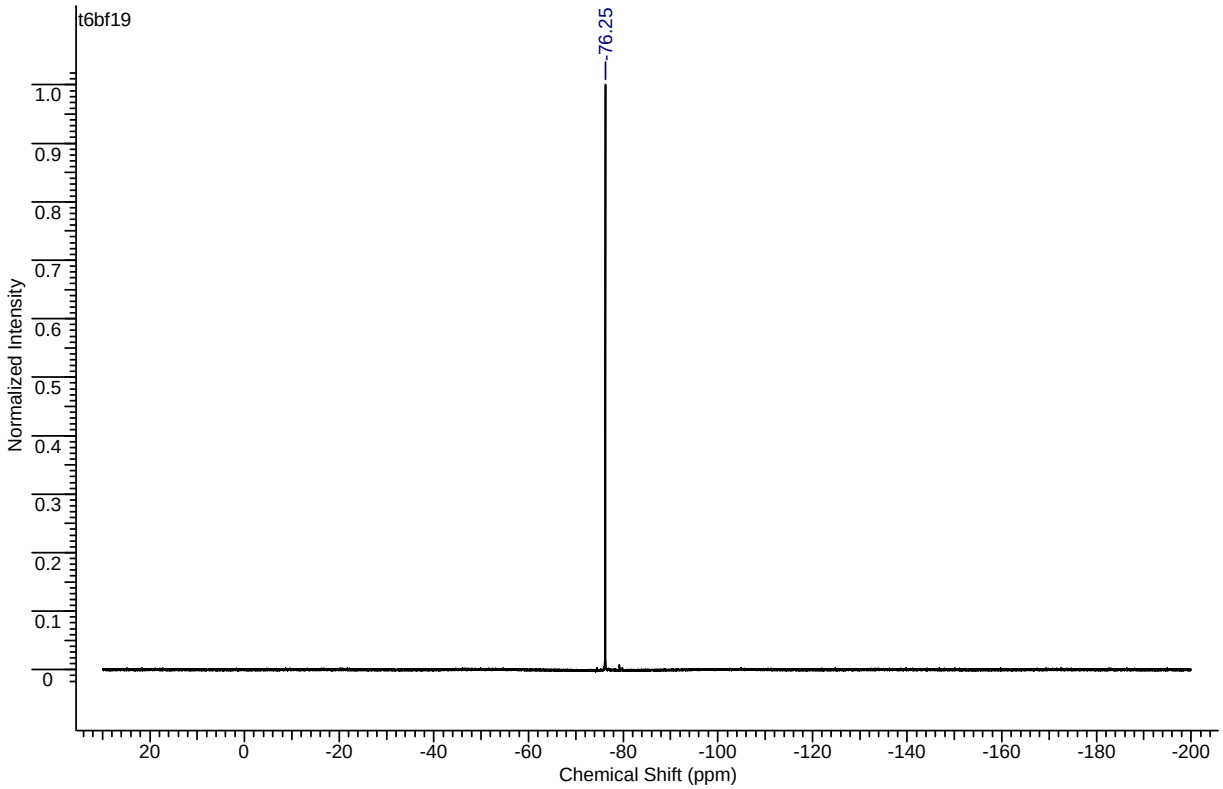

Figure S-5: Room Temperature ^{19}F NMR of **5** in benzene-d_6.

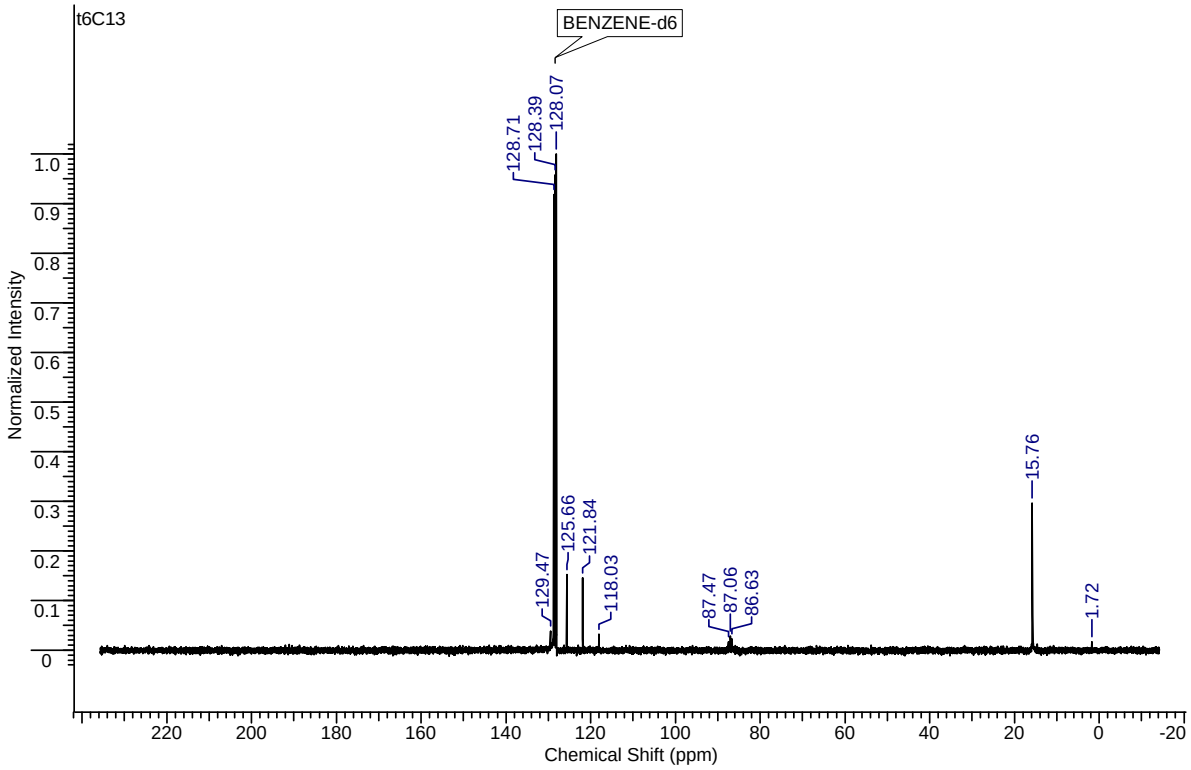

Figure S-6: Room Temperature ^{13}C NMR of **5** in benzene-d_6.

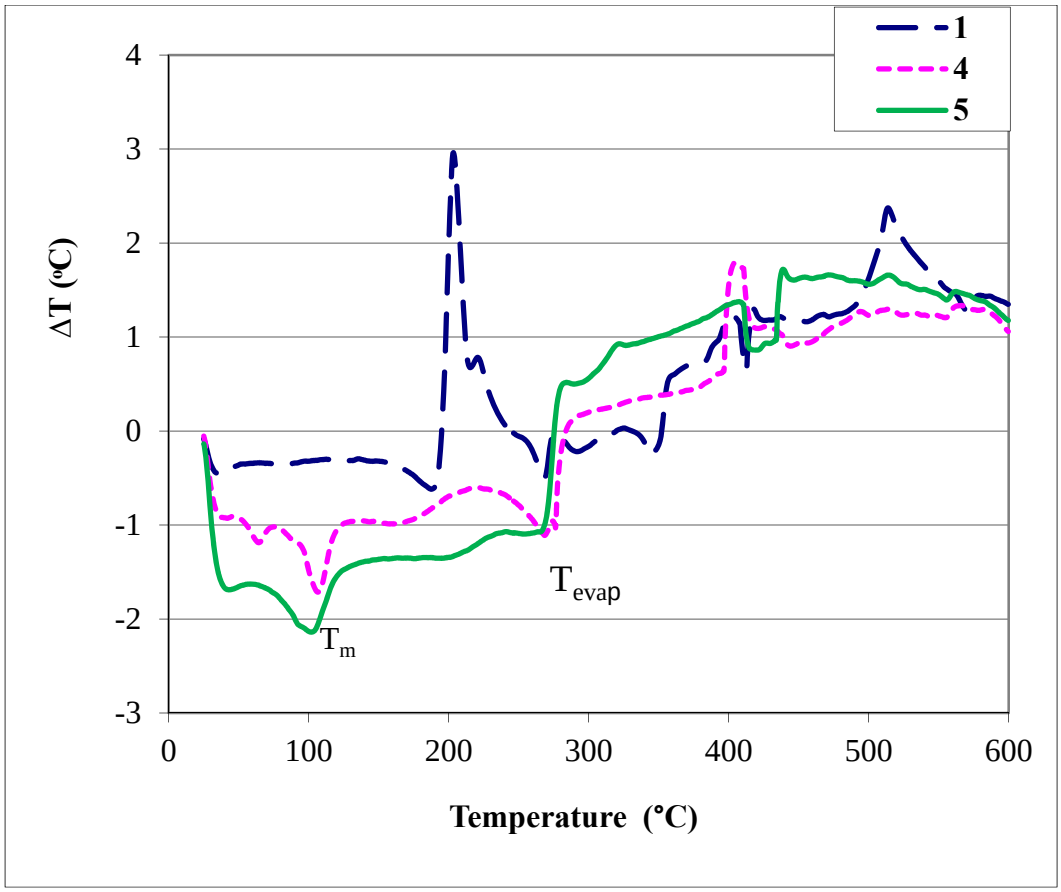

Figure S-7: DTA measurements of compounds **1**, **4** and **5**.

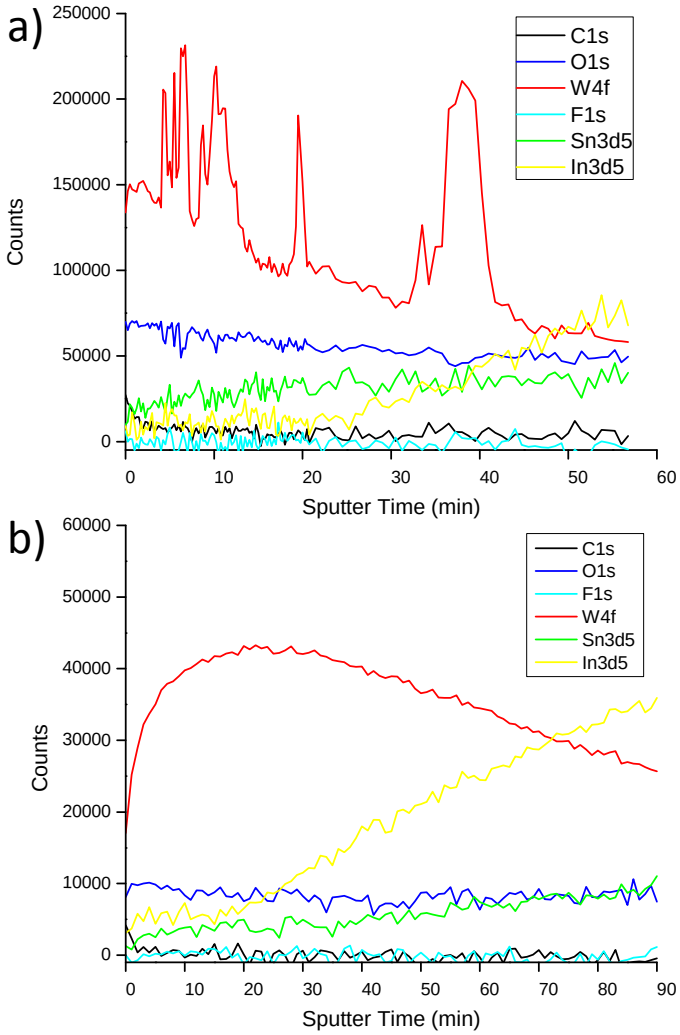

Figure S-8. XPS depth profiles of the films grown at (a) 450 °C and (b) 550 °C. Sputtering performed using 1 keV Ar^+. No F is detected in the film. The variation of the W4f intensity in (a) is most likely due to variations in the densities of the nanorod bundles.

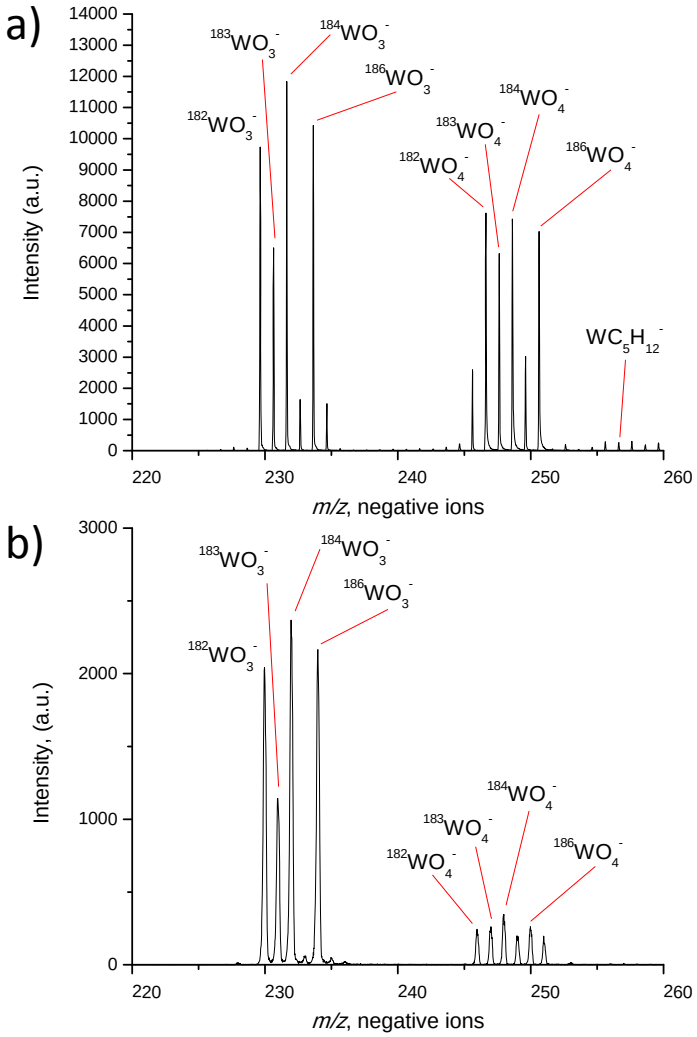

Figure S-9. High mass resolution negative ion spectra centered at m/z 240 for films deposited at 450 °C (a) before and (b) after sputtering for 30s. The data indicate that there are some hydrocarbon species present at the surface.

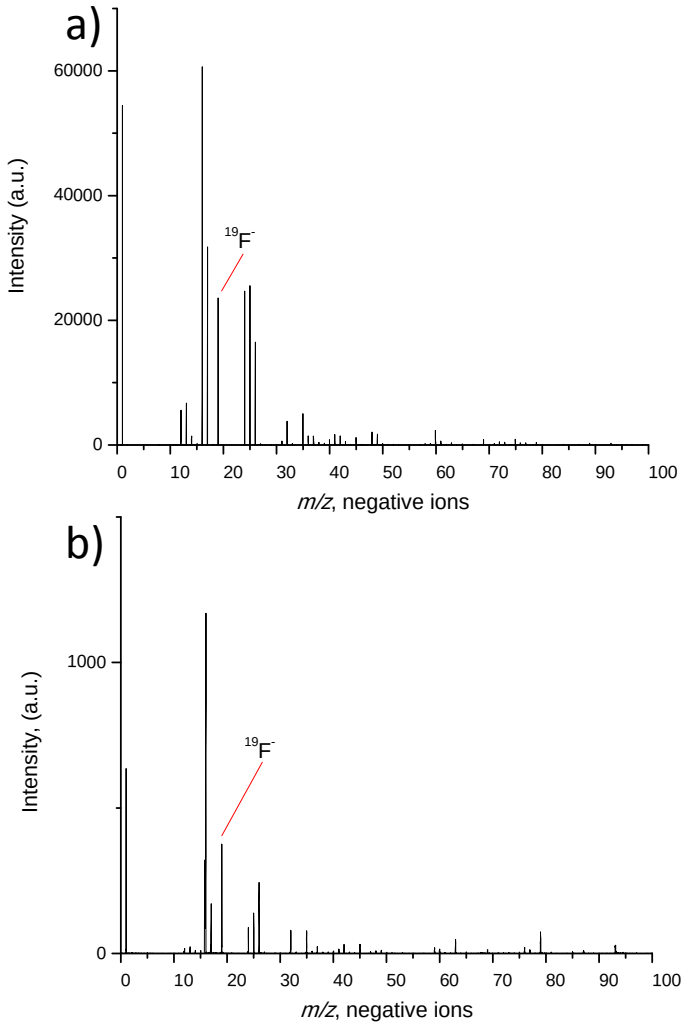

Figure S-10. High mass resolution negative ion spectra *m/z* 0-100 for films deposited at 450 °C (a) before and (b) after sputtering for 30s. The data indicate that there is negligible F present in the deposited films.

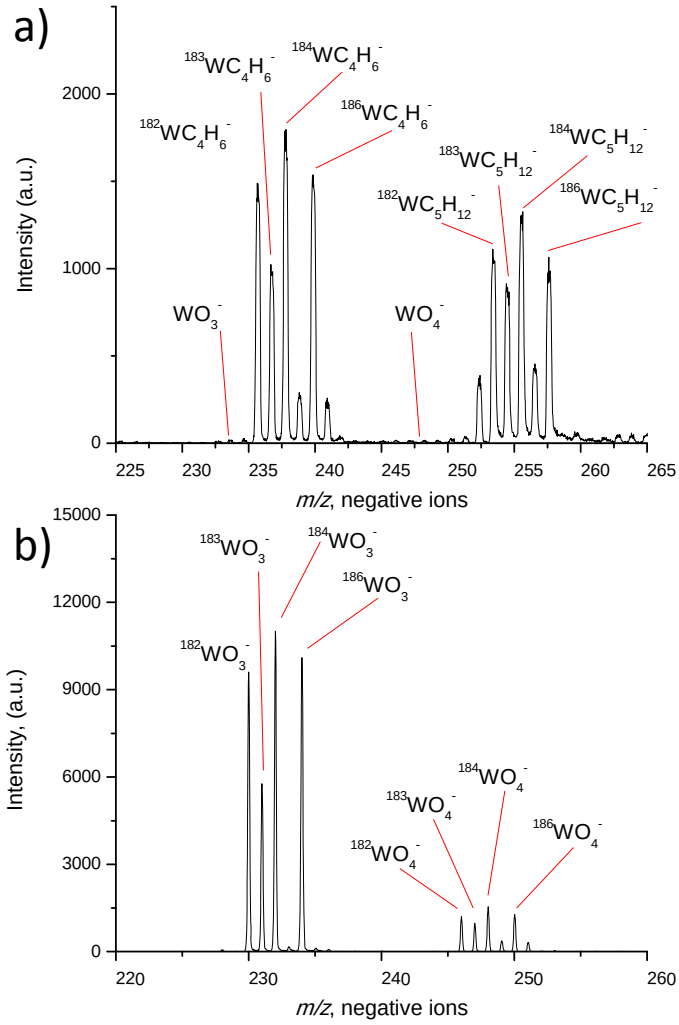

Figure S-11. High mass resolution negative ion spectra centered at *m/z* 240 for films deposited at 550 °C (a) before and (b) after sputtering for 30s. The data indicate that there are hydrocarbon species present at the surface.

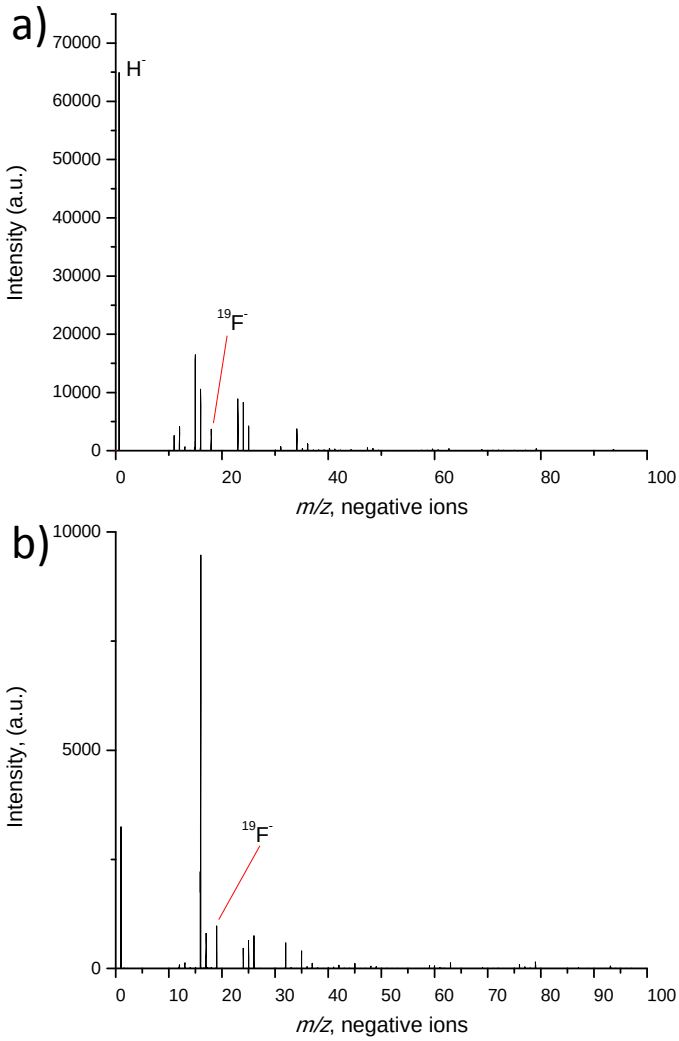

Figure S-12. High mass resolution negative ion spectra m/z 0-100 for films deposited at 550 °C (a) before and (b) after sputtering for 30s. The data indicate that there is negligible F present in the deposited films.

Table S-1: Thermal Behaviors of **1**, **4** and **5** Based on TGA/DTA Measurements.

Compound	Compound Name	T_m, °C	5 % Mass Loss	10 % Mass Loss	% Residue at 600 °C
1	$WOCl_4$	-	173.3	190	15.3
4	$[CF_3(CH_3)_2CO]_4WO$	105.0	172.6	202.5	14.2
5	$[(CF_3)_2CH_3CO]_4WO$	100.5	166.2	199.81	13.6

Table S-2: Relative Abundances for Positive Ion DIPCI Mass Spectra of Complexes **4** and **5**.

Compound	Ion	m/z	rel. abundance (%)[a]
4	$[M]^+$	708	0.05
	$[WO(OC(CH_3)_2CF_3)_3]^+$	581	2
	$[WO(OC(CH_3)_2CF_3)_2(OH)(H_2O)]^+$	489	1
	$[WO(OH)_3(H_2O)+H]^+$	270	1
	$[HOC(CH_3)_2CF_3+H]^+$	129	33
	$[HOC(CH_3)_2CF_3]^+$	128	18
	$[OC(CH_3)_2CF_3]^+$	127	9
	$[HC(CH_3)_2CF_3+H]^+$	113	10
	$[OCH_3CF_3+H]^+$	113	9
	$[OCCH_3CF_3]^+$	112	6
	$[C(CH_3)_2CF_3]^+$	111	12
	$[H_2CCCH_3CF_3]^+$	110	9
	$[HCCCH_3CF_3]^+$	109	100
5	$[M+H]^+$	925	1
	$[M]^+$	924	9
	$[WO(OCCH_3(CF_3)_2)_3]^+$	743	9
	$[WO(OCCH_3(CF_3)_2)_3+2H]^+$	745	1
	$[WO(OCCH_3(CF_3)_2)_2(OH)]^+$	579	12
	$[WO(OH)_3(H_2O)+H]^+$	270	1
	$[HOC_4H_3F_6+H]^+$	183	100
	$[OCCH_3(CF_3)_2]^+$	181	77
	$[H_2CC(CF_3)_2]^+$	164	5
	$HCC(CF_3)_2]^+$	163	51
	$[H_2C(CF_3)_2]^+$	152	39
	$[OCCH_3CF_3+H]^+$	113	28

[a] Relative abundances were predicted by adjusting peak intensities relative to the highest peak normalized to 100 %.

Table S-3: Atomic coordinates (x 10^4) and equivalent isotropic displacement parameters ($Å^2$x 10^3) for **4**. U(eq) is defined as one third of the trace of the orthogonalized U^{ij} tensor.

	x	y	z	U(eq)
W1	0	2660(1)	2500	11(1)
F1	-260(1)	-191(3)	4148(1)	26(1)
F2	-283(1)	3103(3)	4553(1)	24(1)
F3	-1196(1)	920(3)	4322(1)	26(1)
F4	1904(1)	6888(4)	3397(1)	33(1)
F5	2333(1)	3599(4)	3672(1)	30(1)
F6	2408(1)	5963(3)	4479(1)	26(1)
O1	0	-167(5)	2500	21(1)
O2	-405(1)	3138(3)	3185(1)	15(1)
O3	867(1)	3713(4)	3159(1)	22(1)
C1	-1004(1)	2473(5)	3350(1)	15(1)
C2	-679(2)	1571(5)	4098(1)	16(1)
C3	-1454(2)	4527(6)	3330(2)	25(1)
C4	-1437(2)	636(6)	2864(2)	22(1)
C5	1256(1)	4434(5)	3859(1)	14(1)
C6	1976(2)	5221(5)	3851(2)	18(1)
C7	1384(2)	2516(5)	4364(2)	26(1)
C8	877(2)	6383(5)	4037(2)	21(1)

Table S-4: Bond lengths [Å] and angles [°] for **4**.

W1-O1	1.700(3)
W1-O3	1.8718(19)
W1-O3#1	1.8718(19)
W1-O2	1.8995(18)
W1-O2#1	1.8995(18)
F1-C2	1.335(3)
F2-C2	1.342(3)
F3-C2	1.347(3)
F4-C6	1.341(4)
F5-C6	1.342(3)
F6-C6	1.335(3)
O2-C1	1.429(3)
O3-C5	1.425(3)
C1-C4	1.523(4)
C1-C3	1.523(4)
C1-C2	1.529(4)
C3-H3A	0.9800
C3-H3B	0.9800
C3-H3C	0.9800
C4-H4A	0.9800
C4-H4B	0.9800
C4-H4C	0.9800
C5-C7	1.508(4)
C5-C8	1.517(4)
C5-C6	1.531(4)
C7-H7A	0.9800
C7-H7B	0.9800
C7-H7C	0.9800
C8-H8A	0.9800
C8-H8B	0.9800
C8-H8C	0.9800
O1-W1-O3	109.74(7)
O1-W1-O3#1	109.74(7)

O3-W1-O3#1	140.51(15)
O1-W1-O2	98.70(6)
O3-W1-O2	87.33(8)
O3#1-W1-O2	86.82(8)
O1-W1-O2#1	98.70(6)
O3-W1-O2#1	86.82(8)
O3#1-W1-O2#1	87.33(8)
O2-W1-O2#1	162.60(13)
C1-O2-W1	140.54(17)
C5-O3-W1	147.55(17)
O2-C1-C4	111.8(2)
O2-C1-C3	108.3(2)
C4-C1-C3	112.5(2)
O2-C1-C2	105.1(2)
C4-C1-C2	109.1(2)
C3-C1-C2	109.8(2)
F1-C2-F2	107.4(2)
F1-C2-F3	107.0(2)
F2-C2-F3	106.9(2)
F1-C2-C1	112.1(2)
F2-C2-C1	112.2(2)
F3-C2-C1	110.9(2)
C1-C3-H3A	109.5
C1-C3-H3B	109.5
H3A-C3-H3B	109.5
C1-C3-H3C	109.5
H3A-C3-H3C	109.5
H3B-C3-H3C	109.5
C1-C4-H4A	109.5
C1-C4-H4B	109.5
H4A-C4-H4B	109.5
C1-C4-H4C	109.5
H4A-C4-H4C	109.5
H4B-C4-H4C	109.5
O3-C5-C7	110.6(2)

O3-C5-C8	110.1(2)
C7-C5-C8	113.2(2)
O3-C5-C6	104.1(2)
C7-C5-C6	109.2(2)
C8-C5-C6	109.2(2)
F6-C6-F4	106.7(2)
F6-C6-F5	106.7(2)
F4-C6-F5	106.2(2)
F6-C6-C5	111.4(2)
F4-C6-C5	112.6(2)
F5-C6-C5	112.7(3)
C5-C7-H7A	109.5
C5-C7-H7B	109.5
H7A-C7-H7B	109.5
C5-C7-H7C	109.5
H7A-C7-H7C	109.5
H7B-C7-H7C	109.5
C5-C8-H8A	109.5
C5-C8-H8B	109.5
H8A-C8-H8B	109.5
C5-C8-H8C	109.5
H8A-C8-H8C	109.5
H8B-C8-H8C	109.5

Symmetry transformations used to generate equivalent atoms:

#1 -x,y,-z+1/2

Table S-5: Atomic coordinates (x 10^4) and equivalent isotropic displacement parameters ($Å^2$x 10^3) for **5**. U(eq) is defined as one third of the trace of the orthogonalized U^{ij} tensor.

	x	y	z	U(eq)
W(1)	8930(1)	1423(1)	2474(1)	12(1)
S(1)	8077(3)	-756(2)	2261(1)	57(1)
F(1)	7786(4)	773(3)	347(2)	36(1)
F(2)	6791(5)	1843(3)	-159(2)	42(1)
F(3)	5954(5)	1149(3)	736(2)	33(1)
F(4)	6749(5)	3394(3)	556(2)	42(1)
F(5)	5703(4)	2707(3)	1378(2)	31(1)
F(6)	7393(4)	3401(3)	1669(2)	31(1)
F(7)	12507(4)	1329(3)	2120(2)	35(1)
F(8)	13155(5)	587(5)	1212(3)	64(2)
F(9)	11864(6)	1644(4)	1053(3)	49(2)
F(10)	11617(5)	-627(3)	643(3)	50(1)
F(11)	10443(4)	460(3)	357(2)	28(1)
F(12)	9680(5)	-599(3)	968(3)	44(1)
F(13)	5935(5)	3072(3)	2900(2)	42(1)
F(14)	4812(4)	2646(4)	3800(3)	46(1)
F(15)	6759(6)	2976(4)	3957(3)	41(1)
F(16)	4980(4)	993(3)	4220(3)	44(1)
F(17)	6804(4)	1387(4)	4590(2)	35(1)
F(18)	6606(5)	259(3)	3903(2)	40(1)
F(19)	8997(4)	278(3)	4537(2)	39(1)
F(20)	10642(4)	626(3)	5139(2)	42(1)
F(21)	10771(5)	-255(3)	4232(3)	41(1)
F(22)	12326(4)	1704(3)	4496(2)	33(1)
F(23)	12453(4)	790(3)	3606(2)	31(1)
F(24)	11941(4)	2132(3)	3403(2)	31(1)
O(1)	9603(4)	2433(2)	2465(3)	21(1)
O(2)	7797(4)	1613(3)	1667(2)	16(1)
O(3)	10028(5)	831(4)	1829(3)	22(1)
O(4)	7590(4)	1664(3)	3121(2)	23(1)
O(5)	9896(4)	982(3)	3285(3)	16(1)

O(6)	7988(5)	108(3)	2542(3)	41(1)
C(1)	7696(6)	2088(4)	1016(3)	19(1)
C(2)	8950(7)	2388(4)	701(3)	23(1)
C(3)	7040(7)	1461(6)	481(3)	26(2)
C(4)	6874(8)	2900(5)	1154(4)	27(2)
C(5)	11064(6)	340(4)	1612(3)	19(1)
C(6)	11438(6)	-347(4)	2164(4)	27(2)
C(7)	12156(7)	977(6)	1491(4)	28(2)
C(8)	10710(8)	-105(5)	882(4)	28(2)
C(9)	6324(5)	1635(5)	3329(3)	21(1)
C(10)	5447(6)	1272(5)	2734(3)	28(2)
C(11)	5975(8)	2591(5)	3501(4)	29(2)
C(12)	6176(7)	1056(5)	4019(4)	28(2)
C(13)	10381(6)	1256(4)	3961(3)	16(1)
C(14)	9737(6)	2069(4)	4273(3)	22(1)
C(15)	10204(7)	460(5)	4474(4)	25(2)
C(16)	11781(6)	1460(6)	3869(3)	23(1)
C(17)	7390(12)	-1457(6)	2915(5)	63(3)
C(18)	7001(14)	-833(9)	1494(8)	90(4)

Table S-6: Bond lengths [Å] and angles [°] for **5**.

W(1)-O(1)	1.695(4)
W(1)-O(4)	1.888(5)
W(1)-O(3)	1.888(5)
W(1)-O(5)	1.924(5)
W(1)-O(2)	1.927(4)
W(1)-O(6)	2.242(4)
S(1)-O(6)	1.415(6)
S(1)-C(17)	1.762(8)
S(1)-C(18)	1.814(13)
F(1)-C(3)	1.335(9)
F(2)-C(3)	1.334(8)
F(3)-C(3)	1.331(9)
F(4)-C(4)	1.334(8)
F(5)-C(4)	1.341(10)
F(6)-C(4)	1.332(9)
F(7)-C(7)	1.324(8)
F(8)-C(7)	1.318(9)
F(9)-C(7)	1.330(9)
F(10)-C(8)	1.322(9)
F(11)-C(8)	1.320(9)
F(12)-C(8)	1.337(9)
F(13)-C(11)	1.324(8)
F(14)-C(11)	1.353(9)
F(15)-C(11)	1.317(10)
F(16)-C(12)	1.324(8)
F(17)-C(12)	1.337(8)
F(18)-C(12)	1.314(9)
F(19)-C(15)	1.315(8)
F(20)-C(15)	1.327(8)
F(21)-C(15)	1.321(9)
F(22)-C(16)	1.338(7)
F(23)-C(16)	1.334(9)
F(24)-C(16)	1.343(9)
O(2)-C(1)	1.399(7)

O(3)-C(5)	1.387(8)
O(4)-C(9)	1.396(7)
O(5)-C(13)	1.404(7)
C(1)-C(2)	1.521(9)
C(1)-C(4)	1.535(10)
C(1)-C(3)	1.536(9)
C(2)-H(2A)	0.9800
C(2)-H(2B)	0.9800
C(2)-H(2C)	0.9800
C(5)-C(6)	1.507(8)
C(5)-C(7)	1.528(10)
C(5)-C(8)	1.544(9)
C(6)-H(6A)	0.9800
C(6)-H(6B)	0.9800
C(6)-H(6C)	0.9800
C(9)-C(11)	1.533(10)
C(9)-C(10)	1.536(8)
C(9)-C(12)	1.550(9)
C(10)-H(10A)	0.9800
C(10)-H(10B)	0.9800
C(10)-H(10C)	0.9800
C(13)-C(14)	1.525(9)
C(13)-C(16)	1.527(8)
C(13)-C(15)	1.546(9)
C(14)-H(14A)	0.9800
C(14)-H(14B)	0.9800
C(14)-H(14C)	0.9800
C(17)-H(17A)	0.9800
C(17)-H(17B)	0.9800
C(17)-H(17C)	0.9800
C(18)-H(18A)	0.9800
C(18)-H(18B)	0.9800
C(18)-H(18C)	0.9800
O(1)-W(1)-O(4)	98.5(2)

O(1)-W(1)-O(3)	99.6(2)
O(4)-W(1)-O(3)	161.9(2)
O(1)-W(1)-O(5)	95.8(2)
O(4)-W(1)-O(5)	89.2(2)
O(3)-W(1)-O(5)	89.3(2)
O(1)-W(1)-O(2)	96.8(2)
O(4)-W(1)-O(2)	89.0(2)
O(3)-W(1)-O(2)	88.6(2)
O(5)-W(1)-O(2)	167.42(19)
O(1)-W(1)-O(6)	177.0(2)
O(4)-W(1)-O(6)	78.6(2)
O(3)-W(1)-O(6)	83.3(2)
O(5)-W(1)-O(6)	83.3(2)
O(2)-W(1)-O(6)	84.1(2)
O(6)-S(1)-C(17)	106.7(4)
O(6)-S(1)-C(18)	107.4(5)
C(17)-S(1)-C(18)	103.1(6)
C(1)-O(2)-W(1)	141.2(4)
C(5)-O(3)-W(1)	157.7(4)
C(9)-O(4)-W(1)	152.8(4)
C(13)-O(5)-W(1)	140.5(4)
S(1)-O(6)-W(1)	141.3(4)
O(2)-C(1)-C(2)	114.3(5)
O(2)-C(1)-C(4)	108.7(5)
C(2)-C(1)-C(4)	108.5(6)
O(2)-C(1)-C(3)	104.9(5)
C(2)-C(1)-C(3)	110.0(5)
C(4)-C(1)-C(3)	110.3(6)
C(1)-C(2)-H(2A)	109.5
C(1)-C(2)-H(2B)	109.5
H(2A)-C(2)-H(2B)	109.5
C(1)-C(2)-H(2C)	109.5
H(2A)-C(2)-H(2C)	109.5
H(2B)-C(2)-H(2C)	109.5
F(3)-C(3)-F(2)	107.0(6)

F(3)-C(3)-F(1)	107.3(7)
F(2)-C(3)-F(1)	107.4(6)
F(3)-C(3)-C(1)	113.0(5)
F(2)-C(3)-C(1)	112.3(7)
F(1)-C(3)-C(1)	109.6(5)
F(6)-C(4)-F(4)	107.4(6)
F(6)-C(4)-F(5)	107.0(6)
F(4)-C(4)-F(5)	106.5(6)
F(6)-C(4)-C(1)	110.0(6)
F(4)-C(4)-C(1)	112.1(6)
F(5)-C(4)-C(1)	113.6(6)
O(3)-C(5)-C(6)	113.0(5)
O(3)-C(5)-C(7)	107.5(5)
C(6)-C(5)-C(7)	109.8(6)
O(3)-C(5)-C(8)	107.0(6)
C(6)-C(5)-C(8)	109.9(5)
C(7)-C(5)-C(8)	109.6(5)
C(5)-C(6)-H(6A)	109.5
C(5)-C(6)-H(6B)	109.5
H(6A)-C(6)-H(6B)	109.5
C(5)-C(6)-H(6C)	109.5
H(6A)-C(6)-H(6C)	109.5
H(6B)-C(6)-H(6C)	109.5
F(8)-C(7)-F(7)	107.0(6)
F(8)-C(7)-F(9)	107.3(7)
F(7)-C(7)-F(9)	106.3(6)
F(8)-C(7)-C(5)	112.4(7)
F(7)-C(7)-C(5)	110.1(6)
F(9)-C(7)-C(5)	113.3(6)
F(11)-C(8)-F(10)	107.8(6)
F(11)-C(8)-F(12)	106.0(6)
F(10)-C(8)-F(12)	107.2(6)
F(11)-C(8)-C(5)	113.4(6)
F(10)-C(8)-C(5)	111.9(6)
F(12)-C(8)-C(5)	110.1(6)

O(4)-C(9)-C(11)	105.0(6)
O(4)-C(9)-C(10)	113.7(5)
C(11)-C(9)-C(10)	110.0(6)
O(4)-C(9)-C(12)	109.7(5)
C(11)-C(9)-C(12)	110.3(5)
C(10)-C(9)-C(12)	108.2(5)
C(9)-C(10)-H(10A)	109.5
C(9)-C(10)-H(10B)	109.5
H(10A)-C(10)-H(10B)	109.5
C(9)-C(10)-H(10C)	109.5
H(10A)-C(10)-H(10C)	109.5
H(10B)-C(10)-H(10C)	109.5
F(15)-C(11)-F(13)	107.5(7)
F(15)-C(11)-F(14)	107.0(6)
F(13)-C(11)-F(14)	105.8(7)
F(15)-C(11)-C(9)	113.6(6)
F(13)-C(11)-C(9)	111.2(5)
F(14)-C(11)-C(9)	111.2(7)
F(18)-C(12)-F(16)	108.1(7)
F(18)-C(12)-F(17)	107.5(6)
F(16)-C(12)-F(17)	106.8(6)
F(18)-C(12)-C(9)	111.0(6)
F(16)-C(12)-C(9)	111.4(6)
F(17)-C(12)-C(9)	111.9(6)
O(5)-C(13)-C(14)	114.0(5)
O(5)-C(13)-C(16)	108.6(5)
C(14)-C(13)-C(16)	108.3(6)
O(5)-C(13)-C(15)	105.0(5)
C(14)-C(13)-C(15)	110.8(5)
C(16)-C(13)-C(15)	110.2(5)
C(13)-C(14)-H(14A)	109.5
C(13)-C(14)-H(14B)	109.5
H(14A)-C(14)-H(14B)	109.5
C(13)-C(14)-H(14C)	109.5
H(14A)-C(14)-H(14C)	109.5

H(14B)-C(14)-H(14C)	109.5
F(19)-C(15)-F(21)	107.4(7)
F(19)-C(15)-F(20)	107.6(6)
F(21)-C(15)-F(20)	107.8(6)
F(19)-C(15)-C(13)	109.7(6)
F(21)-C(15)-C(13)	112.7(6)
F(20)-C(15)-C(13)	111.4(6)
F(23)-C(16)-F(22)	106.9(6)
F(23)-C(16)-F(24)	106.7(5)
F(22)-C(16)-F(24)	106.2(6)
F(23)-C(16)-C(13)	113.9(6)
F(22)-C(16)-C(13)	112.4(5)
F(24)-C(16)-C(13)	110.3(6)
S(1)-C(17)-H(17A)	109.5
S(1)-C(17)-H(17B)	109.5
H(17A)-C(17)-H(17B)	109.5
S(1)-C(17)-H(17C)	109.5
H(17A)-C(17)-H(17C)	109.5
H(17B)-C(17)-H(17C)	109.5
S(1)-C(18)-H(18A)	109.5
S(1)-C(18)-H(18B)	109.5
H(18A)-C(18)-H(18B)	109.5
S(1)-C(18)-H(18C)	109.5
H(18A)-C(18)-H(18C)	109.5
H(18B)-C(18)-H(18C)	109.5